Journal of Asian Earth Sciences 34 (2009) 258–274

Contents lists available at ScienceDirect

Journal of Asian Earth Sciences

journal homepage: www.elsevier.com/locate/jaes

Nature and processes of the lithospheric mantle beneath the western Qinling: Evidence from deformed peridotitic xenoliths in Cenozoic kamafugite from Haoti, Gansu Province, China

Ben-Xun Su *, Hong-Fu Zhang, Ji-Feng Ying, Yan Xiao, Xin-Miao Zhao

State Key Laboratory of Lithospheric Evolution, Institute of Geology and Geophysics, Chinese Academy of Sciences, P.O. Box 9825, Beijing 100029, China

ARTICLE INFO

Article history:
Received 26 July 2007
Received in revised form 26 May 2008
Accepted 30 May 2008

Keywords:
Cenozoic kamafugite
Deformed peridotite
Lithospheric mantle
Melt pocket
Western Qinling

ABSTRACT

The Cenozoic Haoti kamafugite field (23 Ma) is situated at the western Qinling Orogen, Gansu Province in China, which is a conjunction region of the North China Craton, the Yangtze Craton and the Tibetan Plateau. Fresh peridotitic xenoliths entrained in these volcanic rocks provide an opportunity to study the nature and processes of the lithospheric mantle beneath the western Qinling. These xenoliths can be divided into two groups based on the petrological features and mineral compositions, type 1 and type 2. Type 1 xenoliths with strongly deformed texture have higher Fo (90–92.5) contents in olivines, Mg# (91–94) and Cr# (15–35) of clinopyroxenes, and Cr# (36–67) of spinels than the weakly deformed type 2 xenoliths, which have the corresponding values of 89–90, 89–91.5, 10–15 and 5–15 in minerals, respectively. CaO contents in fine-grained olivines are slightly higher than 0.10 wt% compared with coarse-grained ones (less than 0.10 wt%). Fine-grained clinopyroxenes have low Al_2O_3 + CaO contents (generally <23 wt%) relative to coarse-grained ones (>23 wt%). Fo contents in fine-grained olivines mainly in the melt pocket of the type 1 xenoliths are higher than those in coarse-grained ones, which is somewhat contrary to the type 2 xenoliths without melt pocket. Clinopyroxenes of the type 2 display higher Na_2O contents (1.7–1.9 wt%) than those of the type 1 (<1.4 wt%). P–T estimations reveal that the type 1 xenoliths give temperature in range of 1106–1187 °C and pressure of 21–26 kbar and that relatively low temperature (907 and 1022 °C) and pressure (19.0 and 18.5 kbar) for the type 2 xenoliths. The type 1 xenoliths are characterized by depletion due to high degree of partial melting (>10%), modal metasomatic and deformed characteristics, and may represent the old refractory lithospheric mantle. In contrast, the type 2 peridotites show fertile features with low degree of partial melting (<5%) and may represent the newly-accreted lithospheric mantle. The lithospheric mantle beneath the western Qinling underwent partial melting, recrystallization, deformation and metasomatism due to asthenospheric upwelling and the latest decompression responding to the Cenozoic extensive tectonic environment. These processes perhaps are closely related to the evolution of Tibetan Plateau caused by the India-Asian collision.

1. Introduction

Mafic, ultra-mafic and/or alkaline volcanic rocks and their entrained mantle xenoliths are known as samples directly originating from the mantle of the Earth (Lallemant et al., 1980; Ross, 1980; Boyd et al., 1997; Zhang et al., 2001b, 2008; Zhang, 2005a). Therefore, their petrological and geochemical characteristics can be used to study the nature and evolution of the Earth's mantle. Cenozoic kamafugite in the western Qinling, a complicated orogenic belt in central China, contains abundant mantle xenoliths (Yu, 1991; Yu et al., 2000, 2001, 2004; Shi et al., 2003; Su et al., 2007), which provide an opportunity to probe the lithospheric mantle beneath the region. The Qinling orogenic belt was formed as a result of the closure of the Tethyan Ocean and subsequent collision of the North China Craton with the Yangtze Craton since Paleozoic (Deng, 1996; Gao et al., 1996; Zhang et al., 2002; Su et al., 2006a; Zheng et al., 2008). In Cenozoic, N–S trending orogenic belt was developed in an association with the occurrence of fault-bounded basins and magma activities (Yu, 1991). Previous studies were mainly focused on tectonics and host rock of the mantle xenoliths in the western Qinling (Deng, 1996; Gao et al., 1996; Zhang et al., 2002; Deng, 2003; Yu et al., 2001, 2004). However, little is known about the nature and processes of the lithospheric mantle beneath the western Qinling. Therefore, it is necessary to investigate these peridotitic mantle xenoliths to obtain information on the lithospheric mantle. It is worth to note that there are lots of deformed peridotitic xenoliths among the whole xenolith populations. Deformed mantle xenoliths from orogenic belts are closely related to tectonic movements and/or asthenospheric diapirism (Nicolas et al., 1987;

* Corresponding author. Tel.: +86 10 82998514; fax: +86 10 62010846.
E-mail address: subenxun170@163.com (B.-X. Su).

1367-9120/$ - see front matter
doi:10.1016/j.jseaes.2008.05.009

Witt and Seck, 1987; Bodinier et al., 1990; Tommasi et al., 2008). Compositions of deformed mantle peridotites would vary because of the strong deformation. Thus the compositions of these fresh peridotitic xenoliths can not only give an insight into the nature and evolution of the lithospheric mantle, but also provide implications for tectonic movements and mantle processes.

Lithospheric mantle beneath orogenic belts could be modified many times by tectonic movements and magma activities. Peridotitic xenoliths from the lithospheric mantle beneath orogenic belts have many distinctive characteristics compared with those from the cratons. In this study, we have found many significant features of mantle xenoliths from the western Qinling. These features indicate that all the xenoliths are deformed peridotites and have distinctive compositions between fine-grained and coarse-grained minerals. Detailed mineralogical and petrological studies of the xenoliths are presented with an aim to understand the nature and processes of the lithospheric mantle beneath the western Qinling.

2. Geological setting

The Qinling orogenic belt, an E–W trending mountain range, extends eastward to the Dabie Mountains and westward to the Qilian and Kunlun Mountains (Fig. 1a; Gao et al., 1996; Zhang et al., 2002). The western Qinling Mountains, i.e. the western part of the Qinling orogenic belt, is situated at the northeastern part of the Tibetan Plateau. It is a conjunction region of the North China Craton, the Yangtze Craton and the Tibetan Plateau (Fig. 1a) and can further be divided into the North, Middle and South belts (Zhang et al., 2002). All the three belts have experienced different multi-stage developments from Paleozoic to Cenozoic (Zhang et al., 2002). The tectonic framework in the western Qinling Mountains resulted from a three-direction compression of the ancient Asian Ocean from the north, the Marginal-Pacific Ocean from the southeast and the Paleo-Tethyan Ocean from the southwest (Zhou et al., 2000; Zhang et al., 2001a; Chen et al., 2006). This complicated tectonic characteristic made the Cenozoic fault-bounded basins and deep faults well-developed along NW–SE direction in the region (Zhang et al., 2001a). Late Paleozoic flysches, especially Devonian strata, and Triassic–Jurassic granites outcrop widespread in this region. Paleo-Tethyan ophiolites were discovered in the north margin of the western Qinling (Zhang and Zhou, 2001).

Cenozoic alkaline volcanic rocks in the western Qinling are sparsely distributed in the Lixian, Dangchang and Xihe counties in the Gansu Province (Fig. 1b; Yu, 1991, 1994; Yu et al., 2000). This alkaline volcanic field comprises tens of ultra-mafic volcanic pipes or vent within the Cenozoic Tianshui-Lixian fault basin (Yu, 1994), and coexists with carbonatites. These volcanic rocks intruded into Tertiary sediments, and erupted at 7.1, 7.9, 18.9 and 23 Ma, respectively (Yu, 1994; Liu, 1996; Yu et al., 2005). Geochemical studies of these volcanic rocks show that different episodic eruptions have little compositional differences. These volcanic rocks have SiO_2 contents in the range of 37.7–42.7 wt% and $K_2O + Na_2O$ values of 2.28–7.53 wt% and are classified into kamafugite by Yu (1994).

Kamafugites, extremely rare ultrapotassic, ultramafic lavas outcrop restricted areas including Uganda, Brazil, Italy and China (western Qinling) and always coexist with carbonatites (Foley et al., 1987; Yu, 1994; Lloyd et al., 1996; Sgarbi et al., 2004; D'Orazio et al., 2007). Several kamafugite and carbonatite volcanic pipes outcrop close to Haoti village, Dangchang County in Gansu Province. These volcanic rocks (23 Ma; Yu et al., 2005) have porphyritic, fumarolic and amygdaloidal textures. The phenocrysts include olivine, clinopyroxene and phlogopite with different modes in different layers, and the matrix is eucrystalline, aphanitic, and hyaline with abundant micro-crystal diopside. Abundant mantle xenoliths entrained in the Haoti volcanic rocks are dominantly spinel lherzolites with minor garnet lherzolites, wehrlites, dunites, olivine websterites and clinopyroxenites (Yu, 1991, 1994; Yu et al., 2001, 2004; Shi et al., 2003; Su et al., 2006b, 2007). These xenoliths are small and deformed. Olivine xenocrysts with chemically zoning texture sparsely distributed in the Haoti volcanic rocks (Su et al., 2006b).

3. Xenolith petrology

Mantle xenoliths in this study were collected from the Haoti, Dangchang County in Gansu Province. The xenoliths are fresh and range from 1 to 4 cm in diameter with a few up to 5 or

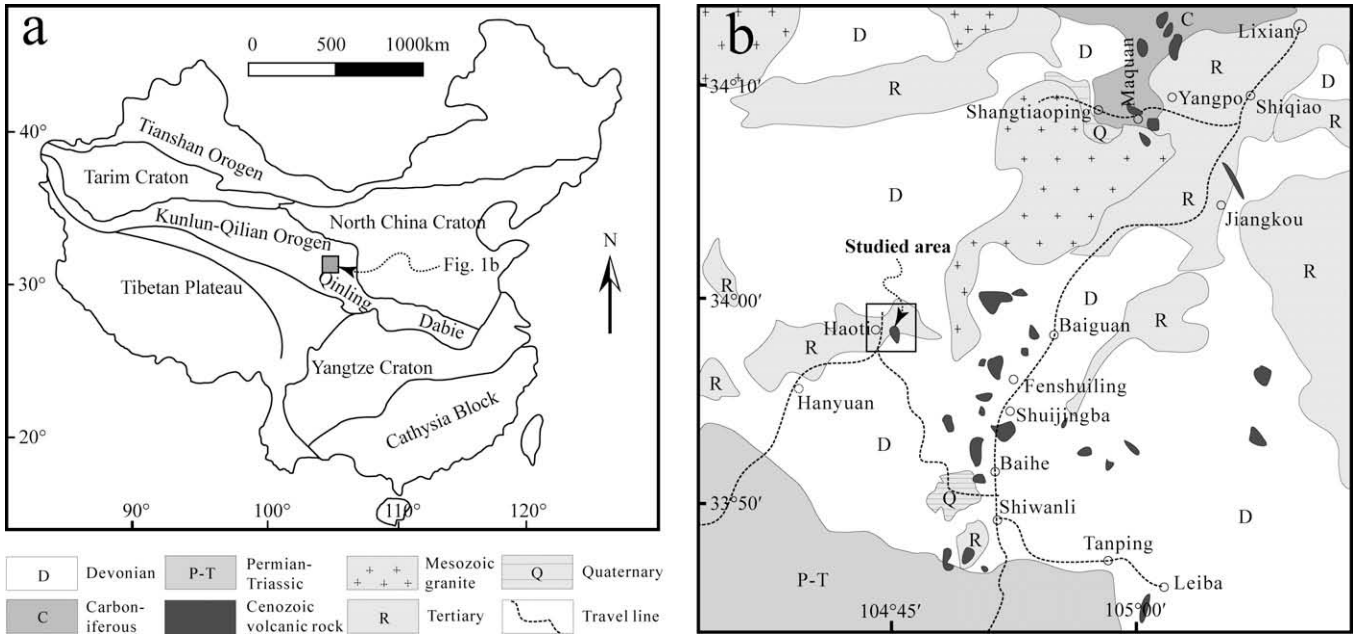

Fig. 1. (a) Schematic tectonic map of China showing major blocks and orogens around the Qinling (modified after Chen et al., 2006 and Yu et al., 2004). (b) The distribution of Cenozoic volcanic rocks in the western Qinling (modified after Yu, 1994 and Yu et al., 2004).

6 cm. Modes of the xenoliths determined by point counting technique are shown in Table 1.

Two groups of mantle peridotitic xenoliths, type 1 and type 2, can be distinguished from mineral compositions as shown below. Haoti spinel lherzolites have high modal olivine (69–84%), moderate modal clinopyroxene (10–18%) and low modal orthopyroxene (8–17%). A feldspar- and ilmenite-bearing spinel lherzolite (HT-24) has the highest modal olivine (80%). The average value (11%) of modal orthopyroxene is similar to those from the North American Proterozoic craton (12%, Schmidberger and Francis, 1999) and typical Phanerozoic peridotites (12.5%, Boyd, 1989), but much lower than that from the Archean Kaapvaal (30%, Boyd, 1989) and Siberia (20%, Boyd et al., 1997) cratons. In the Ol-Opx-Cpx classification diagram (Fig. 2), two samples (HT-10 and HT-44) plot in the wehrlite field, one in the olivine websterite and all others (except HT-24 and HT-15) plot in the lherzolite field and the margin of the field for the on- and off-craton peridotitic xenoliths entrained in the widespread Cenozoic basalts in eastern China (Fan et al., 2000).

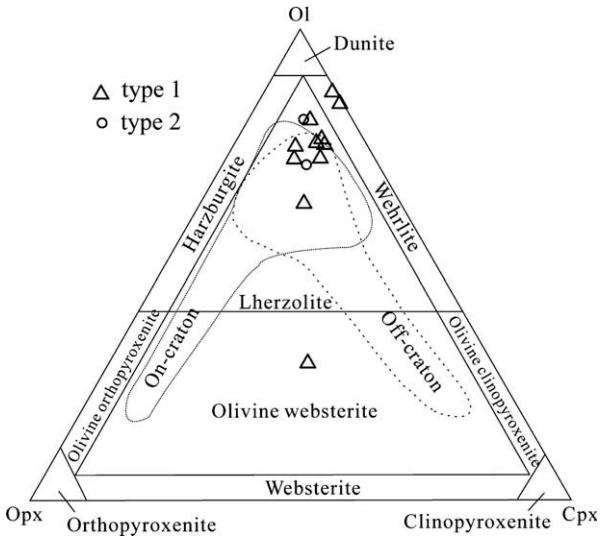

Fig. 2. Petrological classification for the mantle xenoliths from Haoti. The on-craton and off-craton fields are defined by the mantle xenoliths entrained in Cenozoic basalts, eastern China (Fan et al., 2000).

3.1. Type 1

The dominant xenoliths from Haoti are subordinate to the type 1. The type 1 xenoliths exhibit significantly deformed textures with mineral elongation and orientation. The deformation had paralleled the constituent minerals even spinel which is elongated or filled among olivine and pyroxenes (Fig. 3a–d). Coarse-grained olivines and pyroxenes, generally in the range of several mm with a few up to 1–1.5 cm, occur as elongated plates with straight to smoothly curved sub-grain boundaries and display undulose or banded extinction. In particular, some olivine grains are broken into fragments or display plastic and fluidal features (Fig. 3b and d), which can be interpreted as the common sense that olivine is the most abundant but weakest mineral in peridotitic xenoliths (Pearson et al., 2003). Some peridotites (e.g., HT-15, HT-16) show porphyroclastic texture and have olivine and orthopyroxene porphyroclasts set in fine-grained pyroxenes and olivines (Fig. 3e; Fig. 4a and d). Fine-grained olivine and pyroxene are defined as less than 0.1 mm and usually occur as bled and plate among coarse grains and as aggregate in melt pocket (Fig. 3a and c and Fig. 4a and b). Triple junction is found in type 1 xenoliths (Fig. 3c), likely intimating recrystallization, and sometimes is replaced by melt pocket. The melt pockets occur generally among olivine and clinopyroxene grains and sometimes adjacent to orthopyroxenes. These melt pockets are composed of fine-grained olivine and clinopyroxene without glass (Fig. 4a and b). Melt pockets and the absence of glass in them indicate significant partial melting and subsequent recrystallization. In few xenoliths, spinel and garnet show sieved and reaction textures (Fig. 3f and Fig. 4g and h), respectively. The reaction rim of garnet consists of secondary fine-grained clinopyroxene, orthopyroxene and spinel. Feldspar vein cutting through coarse-grained clinopyroxene has been also observed in the Haoti xenoliths (Fig. 4e and f). The presences of phlogopite and disseminated amphibole in clinopyroxene (Fig. 4c) provide evidence of modal metasomatism. These lines of petrological features illustrate that the type 1 xenoliths underwent complex mantle processes involving partial melting, recrystallization, metasomatism due to the fluid/melt-peridotite interaction and deformation.

3.2. Type 2

The type 2 xenoliths including two spinel lherzolites (HT-04 and HT-24) are composed of large, subhedral or anhedral grains

Table 1
Mode of minerals in mantle xenoliths from Haoti, Dangchang County

Sample	Rock type	Mode/%									
		Ol	Cpx	Opx	Sp	Gt	Amp	Phl	Ilm	Feld	Chr
Type 1											
HT-08	Sp lherzolite	74	16	8	2						
HT-15	Sp lherzolite	79	11	8	2						
HT-25	Sp lherzolite	75	15	8	2						
HT-33	Sp lherzolite	71	17	11	1			Trace			Trace
HT-46	Sp lherzolite	73	11	13	3						
HT-16	Sp lherzolite	72	13	15	Trace		Trace	Trace			Trace
HT-23	Lherzolite	76	15	9							
HT-32	Gt lherzolite	63	18	17	Trace	2				Trace	
HT-10	Wehrlite	87	13								
HT-44	Wehrlite	84	16					Trace			Trace
HT-43	Ol websterite	28	35	33	4						
HT-18	Dunite	100									
HT-20	Dunite	99			1						
HT-14	Clinopyroxenite	100					Trace			Trace	
Type 2											
HT-04	Sp lherzolite	69	15	13	3						
HT-24	Sp lherzolite	80	10	9	1				Trace	Trace	

Note: Ol, olivine; Cpx, clinopyroxene; Opx, orthopyroxene; Sp, spinel; Gt: garnet; Amp, amphibole; Phl, phlogopite; Ilm, ilmenite; Feld, feldspar; Chr, chromite.

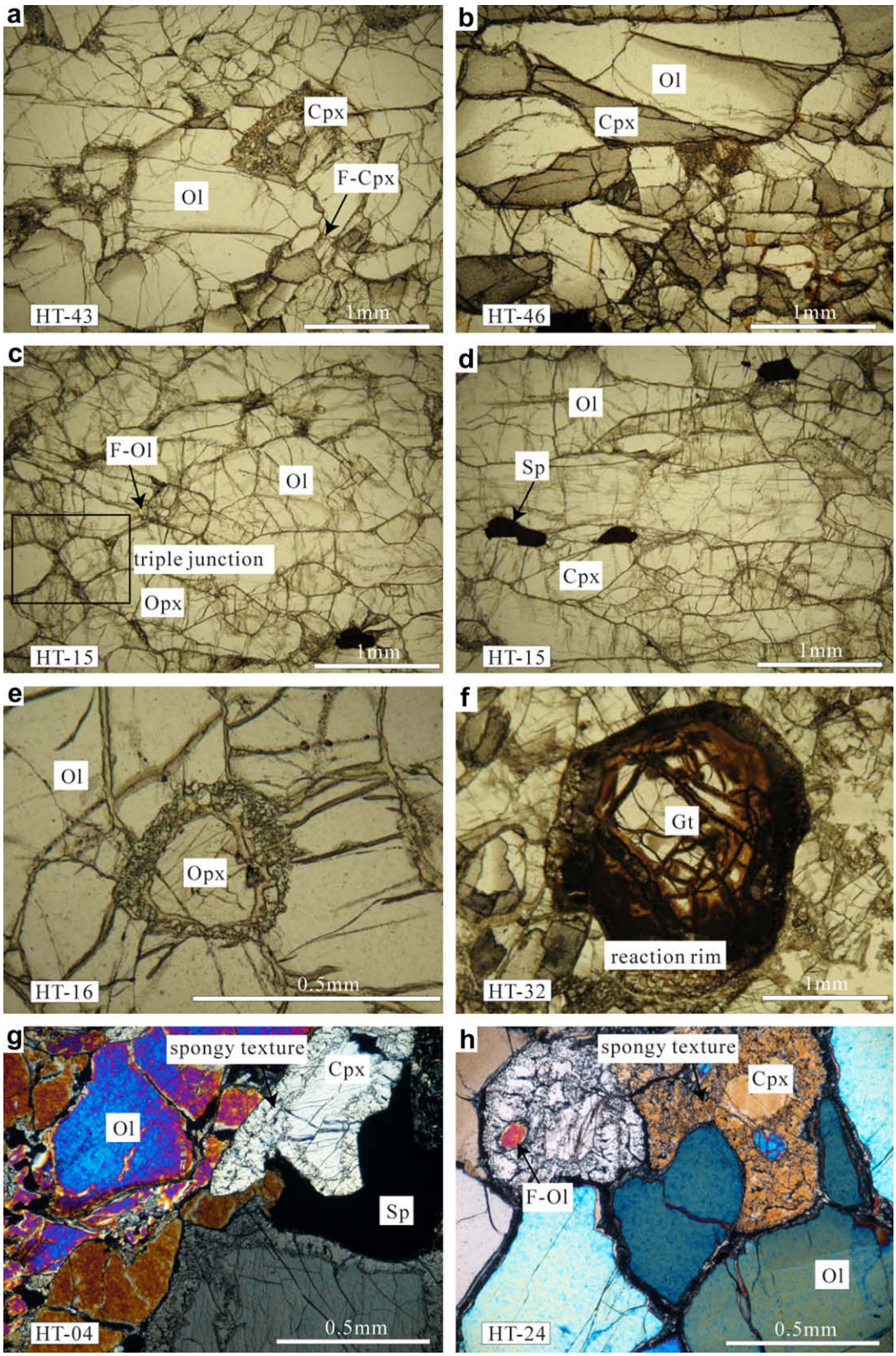

Fig. 3. Photomicrographs of representative peridotitic xenoliths from Haoti. (a) Olivine websterite (HT-43) with porphyroclastic texture and fine-grained clinopyroxene (F-Cpx) present among coarse-grained minerals; (b) spinel lherzolite (HT-46) displaying excellent orientation of elongated minerals; (c) triple junction of minerals and elongated minerals in spinel lherzolite (HT-15); (d) platy metacryst texture in spinel lherzolite (HT-15); (e) porphyroclastic orthopyroxene in spinel lherzolite (HT-16); (f) round and interstitial garnet with reactive texture in garnet lherzolite (HT-32); (g) spinel lherzolite (HT-04) with mechanical comminution of olivine and spongy texture of clinopyroxene; (h) fine-grained olivine occurring as inclusion in clinopyroxene with spongy texture in spinel lherzolite (HT-24).

and show relatively weak deformed texture compared with the type 1 xenoliths. Constituent minerals display wide boundaries and exhibit dominantly mechanical comminution resulting in well-developed cracks/fractures and small chips (Fig. 3g and h)

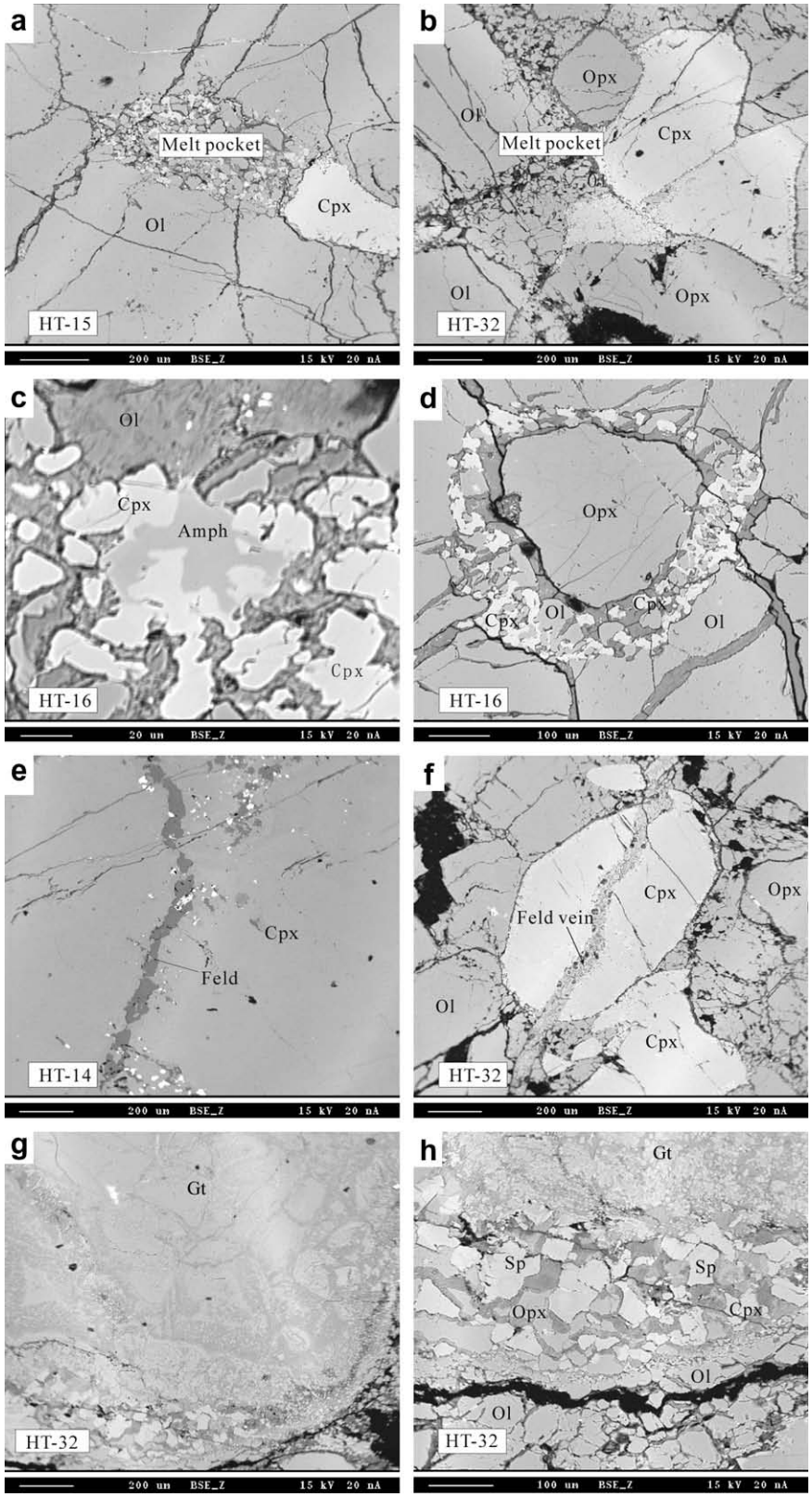

Fig. 4. Backscattered images of peridotitic xenoliths from Haoti. (a) Melt pocket composed of fine-grained olivine and clinopyroxene among coarse-grained olivine and clinopyroxene in spinel lherzolite (HT-15); (b) melt pocket composed of fine-grained olivine and clinopyroxene among coarse-grained olivine, clinopyroxene and orthopyroxene in garnet lherzolite (HT-32); (c) disseminated amphibole in clinopyroxene in spinel lherzolite (HT-16); (d) porphyroclastic orthopyroxene surrounded by fine-grained olivine and clinopyroxene in spinel lherzolite (HT-16); (e) feldspar vein present within clinopyroxene in clinopyroxenite (HT-14); (f) feldspar vein cutting through coarse-grained clinopyroxene in garnet lherzolite (HT-32); (g and h) round garnet showing breakdown texture and phase transition from garnet to spinel in garnet lherzolite (HT-32).

instead of comparable elongation and orientation in the type 1 xenoliths, and the kink band can be observed as well. Most clinopyroxenes have wide-spongy texture and relict parts are still able to be recognized (Fig. 3g and h). Spinels usually occur as anhedral

Table 2
Major element compositions (wt%) of minerals from the Haoti xenoliths

Sample	HT-15								HT-46								
Rock	Sp lherzolite								Sp lherzolite								
Mineral	Ol			Cpx			Opx	Sp	Ol		Cpx			Opx		Sp	
Size	C	C	F-MP	C	F	F-MP	C	F	C	F	C	C	F	C	C	F	F
SiO_2	41.10	41.10	41.10	51.90	54.30	54.00	56.50		41.00	41.30	52.70	52.70	54.30	55.90	55.40		
TiO_2				1.17	0.58	0.84		0.10		0.13	0.08	0.14	0.15			0.22	0.23
Al_2O_3				2.80	0.42	0.74	2.32	21.00			3.32	3.25	0.13	3.09	3.19	27.90	28.10
Cr_2O_3				1.57	1.87	1.93	0.94	49.10		0.14	1.31	1.44	6.40	0.87	0.81	40.90	40.40
FeO	8.52	8.79	8.92	2.87	3.06	2.90	5.36	13.90	8.31	7.62	2.71	2.86	2.06	5.44	5.38	16.30	16.10
MnO	0.12	0.11	0.11	0.09	0.07	0.10	0.14	0.22	0.17	0.22	0.08	0.07	0.13	0.17	0.14		
MgO	48.70	48.70	48.50	16.80	18.50	17.90	33.30	14.90	48.70	49.90	17.80	17.60	15.50	33.00	32.80	3.34	2.89
CaO	0.13	0.11	0.11	20.70	19.20	20.30	1.27	0.02	0.11	0.07	20.50	20.30	17.20	1.20	1.19	0.15	0.09
Na_2O				0.86	1.02	0.99					0.66	0.59	2.95				
NiO	0.43	0.30	0.23	0.05	0.09	0.04	0.15	0.20	0.40	0.24	0.05	0.09	0.00	0.07	0.09	11.30	11.20
Total	99.0	99.1	99.0	98.8	99.2	99.7	100.0	99.3	98.7	99.7	99.2	99.0	98.7	99.7	99.0	100.3	99.3
Oxygen	4	4	4	6	6	6	6	4	4	4	6	6	6	6	6	4	4
Si	1.012	1.011	1.013	1.911	1.983	1.966	1.949		1.012	1.006	1.923	1.926	2.000	1.933	1.930		
Ti				0.032	0.016	0.023		0.002		0.002	0.002	0.004	0.004			0.005	0.006
Al				0.122	0.018	0.032	0.094	0.763			0.143	0.140	0.006	0.126	0.131	1.044	1.061
Cr				0.046	0.054	0.056	0.026	1.197		0.003	0.038	0.042	0.186	0.024	0.022	1.026	1.024
Fe	0.175	0.181	0.184	0.088	0.093	0.088	0.155	0.358	0.171	0.155	0.083	0.087	0.063	0.157	0.157	0.433	0.431
Mn	0.003	0.002	0.002	0.003	0.002	0.003	0.004	0.006	0.004	0.005	0.002	0.002	0.004	0.005	0.004		
Mg	1.787	1.786	1.781	0.922	1.007	0.971	1.712	0.685	1.791	1.812	0.968	0.959	0.851	1.701	1.703	0.158	0.138
Ca	0.003	0.003	0.003	0.817	0.751	0.792	0.047	0.001	0.003	0.002	0.801	0.795	0.679	0.044	0.044	0.005	0.003
Na				0.061	0.072	0.070					0.047	0.042	0.211				
Ni	0.009	0.006	0.005	0.001	0.003	0.001	0.004	0.005	0.008	0.005	0.001	0.003	0.000	0.002	0.003	0.289	0.289
^{IV}Al				0.089	0.017	0.032	0.051				0.077	0.074	0.000	0.067	0.070		
^{VI}Al				0.033	0.001	0.000	0.043				0.065	0.066	0.006	0.059	0.061		
Fe^{3+}				0.011	0.002	0.007	0.000	0.046			0.025	0.000	0.015	0.000	0.000	0.000	0.000
Fe^{2+}				0.077	0.091	0.082	0.155	0.356			0.058	0.087	0.049	0.157	0.157	0.433	0.431
Mg#	91.1	90.8	90.6	91.2	91.5	91.7	91.7	65.6	91.3	92.1	92.1	91.6	93.1	91.5	91.6	97.6	98.3
Cr#				27.4	74.8	63.6		61.1			20.9	23.0	97.1			49.6	49.1
Sample	HT-33								HT-23								
Rock	Sp lherzolite								Lherzolite								
Mineral	Ol			Cpx		Opx	Sp	Chr	Ol		Cpx					Opx	
Size	C	C	F	C	C	C	F	F	C	F	C	C	C	F	F	C	C
SiO_2	40.80	41.10	40.70	52.50	52.30	55.00			40.90	40.70	52.80	52.40	52.70	53.00	54.20	56.10	56.20
TiO_2				0.05	0.06	0.04	0.10	0.47			0.26	0.17	0.13	0.18	0.22	0.15	0.03
Al_2O_3				3.49	3.47	3.63	32.00	0.68			3.16	3.20	2.94	2.92	0.42	2.39	2.24
Cr_2O_3				1.17	1.19	0.83	36.00	63.80			1.08	1.11	0.92	0.99	1.15	0.40	0.37
FeO	8.84	9.00	8.46	3.13	3.01	5.81	12.30	21.50	8.80	9.15	2.25	2.16	2.09	1.95	2.72	5.81	5.91
MnO	0.08	0.08	0.23	0.11	0.09	0.17	0.22	0.40	0.14	0.08	0.12	0.03	0.05	0.03	0.19	0.20	0.15
MgO	48.50	48.20	49.20	17.80	18.00	32.40	16.00	8.39	48.30	48.10	15.90	16.00	16.50	16.20	18.30	33.70	33.40
CaO	0.09	0.11	0.08	20.80	20.90	1.31	0.04	0.11	0.00	0.07	22.30	21.80	22.50	22.00	20.20	0.43	0.35
Na_2O				0.34	0.34					0.06	0.93	0.90	0.88	0.92	0.73		
NiO	0.44	0.35	0.24	0.04	0.10	0.14	0.32	0.03	0.39	0.20	0.08	0.04	0.02	0.04		0.12	0.01
Total	98.7	98.8	98.9	99.5	99.4	99.3	97.0	97.0	98.5	98.4	98.9	97.8	98.8	98.3	98.2	99.2	98.7

(*continued on next page*)

Table 2 (*continued*)

Sample	HT-33								HT-23								
Rock	Sp lherzolite								Lherzolite								
Mineral	Ol			Cpx		Opx	Sp	Chr	Ol		Cpx					Opx	
Size	C	C	F	C	C	C	F	F	C	F	C	C	C	F	F	C	C
Oxygen	4	4	4	6	6	6	4	4	4	4	6	6	6	6	6	6	6
Si	1.009	1.015	1.003	1.915	1.908	1.915			1.012	1.010	1.939	1.941	1.937	1.952	1.996	1.946	1.959
Ti				0.001	0.002	0.001	0.002	0.013			0.007	0.005	0.004	0.005	0.006	0.004	0.001
Al				0.150	0.149	0.149	1.126	0.030			0.137	0.140	0.127	0.127	0.018	0.098	0.092
Cr				0.034	0.034	0.023	0.849	1.859			0.031	0.033	0.027	0.029	0.033	0.011	0.010
Fe	0.183	0.186	0.174	0.095	0.092	0.169	0.307	0.663	0.182	0.190	0.069	0.067	0.064	0.060	0.084	0.169	0.172
Mn	0.002	0.002	0.005	0.003	0.003	0.005	0.006	0.012	0.003	0.002	0.004	0.001	0.002	0.001	0.006	0.006	0.004
Mg	1.787	1.774	1.808	0.968	0.979	1.682	0.712	0.461	1.782	1.780	0.870	0.884	0.904	0.889	1.005	1.743	1.736
Ca	0.002	0.003	0.002	0.813	0.817	0.049	0.001	0.004	0.000	0.002	0.877	0.865	0.886	0.868	0.797	0.016	0.013
Na				0.024	0.024					0.003	0.066	0.065	0.063	0.066	0.052		
Ni	0.009	0.007	0.005	0.001	0.003	0.004	0.008	0.001	0.008	0.004	0.002	0.001	0.001	0.001		0.003	0.000
^{IV}Al				0.085	0.092	0.085					0.061	0.059	0.063	0.048	0.004	0.054	0.041
^{VI}Al				0.065	0.057	0.064					0.076	0.081	0.064	0.079	0.014	0.044	0.052
Fe^{3+}				0.013	0.032	0.000	0.027	0.000			0.009	0.001	0.041	0.000	0.000	0.000	0.000
Fe^{2+}				0.083	0.060	0.169	0.306	0.663			0.060	0.066	0.023	0.060	0.084	0.169	0.172
Mg#	90.7	90.5	91.2	91.0	91.4	90.9	70.0	41.0	90.7	90.4	92.6	93.0	93.3	93.7	92.3	91.2	91.0
Cr#				18.3	18.7		46.6	98.4			18.7	18.9	17.3	18.5	64.4		

Sample	HT-24									HT-43							
Rock	Sp lherzolite									Ol websterite							
Mineral	Ol				Cpx		Opx	Sp	Ilm	Ol		Cpx		Opx		Sp	
Size	C	C	F	F	C	F	C	F	F	C	F	C	C	C	F	C	F
SiO_2	40.70	40.80	40.00	39.40	52.30	52.40	55.00			41.10	40.80	52.80	52.50	55.40	55.10		
TiO_2					0.60	1.78	0.32	0.20	54.10			0.06	0.12	0.02	0.08	0.26	0.26
Al_2O_3				0.31	5.49	0.26	3.61	62.00				3.50	3.54	3.38	3.39	29.70	29.10
Cr_2O_3				0.51	1.16	0.91	0.50	5.56	0.06		0.11	1.39	1.30	0.96	0.85	38.60	39.50
FeO	10.20	10.60	12.20	13.20	3.42	3.60	6.59	11.00	37.30	8.50	7.44	2.71	2.70	5.37	5.33	14.80	15.00
MnO	0.13	0.13	0.41	0.39	0.08	0.11	0.07	0.17	0.93	0.09	0.08	0.11	0.09	0.12	0.13	0.13	0.08
MgO	47.30	47.20	46.00	44.80	15.70	15.80	31.90	20.00	5.76	49.00	49.70	17.70	17.80	32.90	32.80	16.40	16.60
CaO	0.05	0.08	0.51	0.78	18.90	22.50	0.81	0.03	0.03	0.11	0.04	20.30	20.30	1.25	1.22		
Na_2O					1.79	0.90	0.16		0.07			0.56	0.69				
NiO	0.39	0.37	0.17	0.13	0.03	0.01	0.08	0.06	0.03	0.37	0.25	0.10	0.08	0.15	0.11	0.27	0.22
Total	98.8	99.2	99.3	99.6	99.5	98.3	99.0	99.2	98.3	99.1	98.5	99.4	99.1	99.6	99.0	100.3	100.9
Oxygen	4	4	4	4	6	6	6	4	3	4	4	6	6	6	6	4	4
Si	1.012	1.012	1.001	0.991	1.903	1.957	1.922			1.010	1.005	1.924	1.917	1.921	1.920		
Ti					0.016	0.050	0.008	0.004	0.999			0.002	0.003	0.001	0.002	0.006	0.006
Al				0.009	0.235	0.011	0.149	1.877	0.000			0.150	0.152	0.138	0.139	1.033	1.008
Cr				0.010	0.033	0.027	0.014	0.113	0.001		0.002	0.040	0.038	0.026	0.023	0.900	0.918
Fe	0.212	0.220	0.255	0.278	0.104	0.112	0.193	0.236	0.766	0.175	0.153	0.083	0.082	0.156	0.155	0.365	0.369
Mn	0.003	0.003	0.009	0.008	0.002	0.003	0.002	0.004	0.019	0.002	0.002	0.003	0.003	0.004	0.004	0.003	0.002
Mg	1.753	1.745	1.716	1.680	0.851	0.880	1.662	0.766	0.211	1.794	1.825	0.962	0.969	1.701	1.704	0.721	0.728
Ca	0.001	0.002	0.014	0.021	0.737	0.900	0.030	0.001	0.001	0.003	0.001	0.793	0.794	0.046	0.046		
Na					0.126	0.065	0.011		0.003			0.040	0.049				
Ni	0.008	0.007	0.003	0.003	0.001	0.000	0.002	0.002	0.001	0.007	0.005	0.003	0.002	0.004	0.003	0.002	0.002
^{IV}Al					0.097	0.011	0.078					0.076	0.083	0.079	0.080		
^{VI}Al					0.138	0.000	0.071					0.074	0.069	0.059	0.059		
Fe^{3+}					0.029	0.020	0.000	0.000	0.000			0.000	0.028	0.000	0.000	0.000	0.000
Fe^{2+}					0.075	0.093	0.193	0.236	0.766			0.083	0.054	0.156	0.155	0.365	0.369
Mg#	89.2	88.8	87.0	85.8	89.1	88.6	89.6	76.3		91.1	92.3	92.1	92.1	91.6	91.6	66.3	66.4
Cr#					12.4	70.5		5.7				21.1	19.8			46.6	47.7

SiO_2	41.70	41.40	41.50	41.40	41.90	55.20	53.90	53.70	54.20	55.10	56.80	57.20	57.30	57.10		
TiO_2						0.16	0.65	0.30	0.45	0.16					0.73	
Al_2O_3						0.12	0.83	0.23	1.05	0.06	1.66	1.52	1.55	1.56	16.40	0.19
Cr_2O_3						2.50	0.62	2.90	1.46	2.71	0.67	0.60	0.67	0.59	49.70	68.60
FeO	8.14	7.99	8.35	7.22	7.87	2.72	2.65	2.47	2.80	2.20	5.16	5.10	5.18	4.98	17.30	16.60
MnO	0.11	0.10	0.18	0.12	0.12	0.09		0.07	0.07	0.06	0.12	0.15	0.17	0.18	0.37	0.34
MgO	49.80	49.60	49.70	50.00	49.80	19.00	17.10	17.70	18.00	17.50	34.30	34.10	34.50	34.30	14.00	9.93
CaO	0.08	0.03	0.06	0.16	0.10	18.80	23.80	18.80	20.40	20.50	0.85	0.78	0.84	0.85		0.09
Na_2O						1.29	0.58	1.68	1.19	1.31	0.13	0.11	0.09	0.13		
NiO	0.45	0.42	0.34	0.21	0.17	0.05	0.11	0.06	0.09		0.10	0.13	0.11	0.11	0.26	
Total	100.3	99.6	100.1	99.1	99.9	99.9	100.3	98.0	99.7	99.7	99.9	99.8	100.4	99.8	98.9	95.9
Oxygen	4	4	4	4	4	6	6	6	6	6	6	6	6	6	4	4
Si	1.011	1.011	1.009	1.011	1.016	1.996	1.962	1.989	1.971	2.004	1.959	1.972	1.963	1.966		
Ti						0.004	0.018	0.008	0.012	0.004					0.018	
Al						0.005	0.036	0.010	0.045	0.003	0.067	0.062	0.063	0.063	0.619	0.008
Cr						0.071	0.018	0.085	0.042	0.078	0.018	0.016	0.018	0.016	1.258	1.959
Fe	0.165	0.163	0.170	0.147	0.160	0.082	0.081	0.076	0.085	0.067	0.149	0.147	0.148	0.143	0.463	0.501
Mn	0.002	0.002	0.004	0.002	0.002	0.003		0.002	0.002	0.002	0.004	0.004	0.005	0.005	0.010	0.010
Mg	1.800	1.805	1.801	1.820	1.800	1.024	0.928	0.977	0.976	0.949	1.763	1.752	1.762	1.761	0.668	0.535
Ca	0.002	0.001	0.002	0.004	0.003	0.728	0.928	0.746	0.795	0.799	0.031	0.029	0.031	0.031		0.003
Na						0.090	0.041	0.121	0.084	0.092	0.009	0.007	0.006	0.009		
Ni	0.009	0.008	0.007	0.004	0.003	0.001	0.003	0.002	0.003		0.003	0.004	0.003	0.003	0.007	
^{IV}Al						0.004	0.036	0.010	0.029	0.000	0.041	0.028	0.037	0.034		
^{VI}Al						0.001	0.000	0.000	0.016	0.003	0.026	0.033	0.026	0.030		
Fe^{3+}						0.000	0.028	0.000	0.045	0.000	0.008	0.000	0.000	0.000	0.115	0.000
Fe^{2+}						0.082	0.054	0.076	0.040	0.067	0.140	0.147	0.148	0.143	0.457	0.501
Mg#	91.6	91.7	91.4	92.5	91.9	92.6	92.0	92.7	92.0	93.4	92.2	92.3	92.2	92.5	59.0	51.6
Cr#						93.4	33.1	89.4	48.2	96.9					67.0	99.6

Sample	HT-25								HT-32									
Rock	Sp lherzolite								Gt lherzolite									
Mineral	Ol			Cpx		Opx		Sp	Ol			Cpx			Opx		Sp	Gt
Size	C	C	F	C	F	C	F	C	C	F-MP	F-Gt	C	F-MP	F-Gt	C	F-Gt	F-Gt	C
SiO_2	40.80	41.20	41.30	52.40	54.40	55.70	55.30		41.20	40.40	40.10	52.60	52.40	50.30	55.00	53.20		42.80
TiO_2				0.45	0.46	0.18	0.21	0.55		0.22	0.00	0.34	0.38	0.30				0.21
Al_2O_3				4.05	0.18	3.28	3.38	36.60		0.10	0.03	5.66	5.76	8.39	4.20	6.38	58.40	22.40
Cr_2O_3				1.33	3.97	0.69	0.64	30.40		0.13	0.04	1.49	1.42	0.86	0.77	0.46	9.48	2.35
FeO	9.44	9.07	8.29	2.57	2.75	5.60	5.52	13.60	9.34	9.65	9.82	2.65	3.13	3.84	6.02	6.67	9.99	6.84
MnO	0.19	0.14	0.20	0.02	0.11	0.16	0.10	0.27	0.13	0.21	0.20	0.11	0.08	0.26	0.11	0.28	0.17	0.28
MgO	48.70	48.70	49.70	16.60	17.20	32.80	32.90	17.50	48.80	49.20	49.00	16.20	16.30	16.70	32.10	30.70	20.90	21.00
CaO	0.08	0.07	0.07	20.70	18.40	0.70	0.81		0.08	0.22	0.14	18.60	18.80	18.80	0.98	1.61	0.05	5.19
Na_2O				1.10	1.91	0.13	0.08					1.65	1.78	0.94				0.02
NiO	0.29	0.40	0.13	0.06	0.04	0.10	0.05	0.27	0.42	0.54	0.36	0.06	0.05	0.03			0.12	
Total	99.5	99.6	99.7	99.3	99.4	99.3	99.0	99.3	100.0	100.7	99.7	99.3	100.2	100.4	99.2	99.5	99.2	101.1

(*continued on next page*)

Table 2 (*continued*)

Sample	HT-25								HT-32									
Rock	Sp lherzolite								Gt lherzolite									
Mineral	Ol			Cpx		Opx		Sp	Ol			Cpx			Opx		Sp	Gt
Size	C	C	F	C	F	C	F	C	C	F-MP	F-Gt	C	F-MP	F-Gt	C	F-Gt	F-Gt	C
Oxygen	4	4	4	6	6	6	6	4	4	4	4	6	6	6	6	6	4	12
Si	1.004	1.010	1.008	1.912	1.988	1.932	1.925		1.008	0.987	0.989	1.907	1.892	1.815	1.915	1.859		3.001
Ti				0.012	0.013	0.005	0.005	0.012		0.004	0.000	0.009	0.010	0.008	0.000	0.000		0.011
Al				0.174	0.008	0.134	0.139	1.237		0.003	0.001	0.242	0.245	0.357	0.172	0.263	1.784	1.851
Cr				0.038	0.115	0.019	0.018	0.689		0.003	0.001	0.043	0.041	0.025	0.021	0.013	0.194	0.130
Fe	0.194	0.186	0.169	0.078	0.084	0.162	0.161	0.326	0.191	0.197	0.203	0.080	0.095	0.116	0.175	0.195	0.217	0.401
Mn	0.004	0.003	0.004	0.001	0.003	0.005	0.003	0.007	0.003	0.004	0.004	0.003	0.002	0.008	0.003	0.008	0.004	0.017
Mg	1.786	1.780	1.807	0.903	0.937	1.696	1.707	0.748	1.780	1.792	1.802	0.875	0.878	0.898	1.666	1.600	0.808	2.195
Ca	0.002	0.002	0.002	0.809	0.721	0.026	0.030	0.000	0.002	0.006	0.004	0.722	0.728	0.727	0.037	0.060	0.001	0.390
Na				0.078	0.135	0.009	0.005					0.116	0.125	0.066		0.009		0.003
Ni	0.006	0.008	0.003	0.002	0.001	0.003	0.001	0.006	0.008	0.011	0.007	0.002	0.001	0.001	0.000	0.000	0.003	
^{IV}Al				0.088	0.008	0.068	0.075					0.093	0.108	0.185	0.085	0.141		
^{VI}Al				0.086	0.000	0.066	0.063					0.149	0.138	0.171	0.087	0.122		
Fe^{3+}				0.024	0.016	0.000	0.000	0.066				0.000	0.050	0.058	0.000	0.004	0.028	0.000
Fe^{2+}				0.054	0.068	0.162	0.161	0.323				0.080	0.044	0.057	0.175	0.191	0.216	0.401
Mg#	90.2	90.5	91.4	92.0	91.8	91.3	91.4	69.6	90.3	90.1	89.9	91.6	90.3	88.6	90.5	89.1	78.9	84.5
Cr#				18.0	93.5			35.8				15.0	14.2	6.4			9.8	6.6

Sample	HT-04										HT-08							
Rock	Sp lherzolite										Sp lherzolite							
Mineral	Ol			Cpx	Opx	Sp					Ol		Cpx		Opx		Sp	
Size	C	C	F	C	C	C	C-r	C-c	C-r	C-c	C	C	C	C	C	F	C	F
SiO_2	41.30	40.90	41.10	51.90	55.40						41.20	41.00	53.20	53.20	55.70	56.20		
TiO_2				0.44	0.13	1.90	0.18	0.12	0.23	0.95			0.04	0.08			0.20	0.15
Al_2O_3				6.33	4.44	40.40	54.90	54.90	54.70	49.10			2.48	2.51	2.46	2.42	21.80	21.50
Cr_2O_3				0.99	0.45	18.30	13.00	13.30	13.00	13.60			1.16	1.22	0.91	0.88	46.60	46.40
FeO	9.58	9.69	9.80	2.46	6.07	24.90	11.20	11.50	11.70	17.30	9.02	9.39	2.80	2.74	5.56	5.71	11.90	11.80
MnO	0.16	0.16	0.13	0.04	0.09	0.29	0.09	0.06	0.12	0.23	0.20	0.21	0.11	0.13	0.12	0.11	0.12	0.19
MgO	48.50	48.00	48.40	14.80	32.70	15.10	19.70	19.90	19.80	18.90	48.80	48.60	18.10	18.40	33.10	33.10	15.10	15.00
CaO	0.05	0.03	0.05	20.40	0.52						0.12	0.17	20.70	20.50	1.20	1.23		
Na_2O				1.84	0.09								0.39	0.50				
NiO	0.46	0.39	0.37		0.07	0.17	0.34	0.36	0.38	0.44	0.33	0.35	0.03	0.04	0.12	0.15	0.10	0.17
Total	100.1	99.1	99.8	99.3	99.9	101.1	99.3	100.1	100.0	100.5	99.6	99.7	99.0	99.3	99.1	99.7	95.8	95.1
Oxygen	4	4	4	6	6	4	4	4	4	4	4	4	6	6	6	6	4	4
Si	1.011	1.010	1.009	1.892	1.911						1.009	1.006	1.944	1.938	1.940	1.945		
Ti				0.012	0.003	0.041	0.004	0.002	0.005	0.019			0.001	0.002			0.005	0.004
Al				0.272	0.180	1.363	1.705	1.696	1.695	1.569			0.107	0.108	0.101	0.099	0.811	0.806
Cr				0.029	0.012	0.414	0.271	0.276	0.270	0.291			0.034	0.035	0.025	0.024	1.163	1.167
Fe	0.196	0.200	0.201	0.075	0.175	0.596	0.247	0.252	0.257	0.392	0.185	0.193	0.086	0.083	0.162	0.165	0.314	0.314
Mn	0.003	0.003	0.003	0.001	0.003	0.007	0.002	0.001	0.003	0.005	0.004	0.004	0.003	0.004	0.004	0.003	0.003	0.005
Mg	1.769	1.767	1.770	0.804	1.681	0.644	0.774	0.777	0.776	0.764	1.782	1.778	0.986	0.999	1.718	1.708	0.710	0.711
Ca	0.001	0.001	0.001	0.797	0.019						0.003	0.004	0.810	0.800	0.045	0.046	0.000	0.000
Na				0.130	0.006								0.028	0.035				
Ni	0.009	0.008	0.007	0.000	0.002	0.004	0.007	0.008	0.008	0.010	0.007	0.007	0.001	0.001	0.003	0.004	0.003	0.004
^{IV}Al				0.108	0.089								0.056	0.062	0.060	0.055		
^{VI}Al				0.164	0.091								0.051	0.046	0.041	0.044		
Fe^{3+}				0.033	0.000	0.183	0.023	0.032	0.035	0.132			0.000	0.018	0.000	0.000	0.023	0.027
Fe^{2+}				0.041	0.175	0.583	0.246	0.251	0.256	0.386			0.086	0.065	0.162	0.165	0.313	0.313
Mg#	90.0	89.8	89.8	91.5	90.6	51.9	75.9	75.5	75.1	66.0	90.6	90.2	92.0	92.3	91.4	91.2	69.4	69.3
Cr#				9.5		23.3	13.7	14.0	13.7	15.6			24.0	24.7			58.9	59.2

Sample	HT-31			HT-07		HT-14		HT-20				HT-18		HT-44		HT-10		
Rock	Cpx megcryst			Cpx megcryst		Clinopyroxenite		Dunite				Dunite		Wehrlite		Wehrlite		
Mineral	Cpx			Cpx		Cpx		Ol		Sp		Ol		Ol	Cpx	Ol		Cpx
Size	C	F	F	C	C	C	F	C	F	F	F	C	C	C	C	C	F	F
SiO_2	50.90	51.80	51.60	51.10	51.30	46.60	52.60	41.40	41.50			41.20	41.30	41.20	53.70	41.10	41.20	54.00
TiO_2	0.91	0.86	0.87	1.13	1.05	2.96	1.36			0.36	0.35				0.11			
Al_2O_3	7.06	7.04	7.02	7.29	7.10	6.11	0.77			25.90	25.60				2.77			0.17
Cr_2O_3	0.09	0.09	0.05	0.01	0.04	0.36	0.02			42.40	41.40		0.11		2.21			2.81
FeO	6.87	6.84	6.88	7.14	7.09	5.60	4.29	7.26	7.40	13.30	17.10	8.97	9.22	8.71	2.60	8.96	9.56	2.17
MnO	0.22	0.16	0.19	0.16	0.18	0.05	0.12	0.10	0.11	0.03	0.27	0.14	0.13	0.09	0.09	0.14	0.08	0.05
MgO	15.20	15.50	15.40	14.90	15.00	13.10	15.40	49.80	50.00	17.20	14.80	48.90	48.60	48.70	17.60	49.30	49.10	16.50
CaO	16.10	16.10	15.90	16.30	16.40	23.60	24.10	0.09	0.08			0.06	0.07	0.09	18.80	0.08	0.11	21.40
Na_2O	1.87	1.91	1.85	1.90	1.83	0.60	0.52								1.40			1.42
NiO	0.05	0.09	0.07	0.04			0.03	0.42	0.41	0.18	0.14	0.35	0.39	0.43	0.07	0.41	0.39	0.04
Total	99.3	100.4	99.9	100.0	100.1	98.9	99.2	99.0	99.5	99.5	99.8	99.6	99.8	99.2	99.4	99.9	100.4	98.6
Oxygen	6	6	6	6	6	6	6	4	4	4	4	4	4	4	6	4	4	6
Si	1.868	1.877	1.879	1.864	1.870	1.758	1.953	1.012	1.011			1.009	1.011	1.012	1.951	1.004	1.004	1.995
Ti	0.025	0.023	0.024	0.031	0.029	0.084	0.038			0.008	0.008				0.003			
Al	0.305	0.301	0.301	0.313	0.305	0.272	0.034			0.915	0.917				0.119			0.007
Cr	0.003	0.003	0.001	0.000	0.001	0.011	0.001			1.004	0.995		0.002		0.063			0.082
Fe	0.211	0.207	0.210	0.218	0.216	0.177	0.133	0.148	0.151	0.333	0.435	0.184	0.189	0.179	0.079	0.183	0.195	0.067
Mn	0.007	0.005	0.006	0.005	0.006	0.002	0.004	0.002	0.002	0.001	0.007	0.003	0.003	0.002	0.003	0.003	0.002	0.002
Mg	0.832	0.837	0.836	0.810	0.815	0.737	0.852	1.815	1.815	0.768	0.671	1.786	1.774	1.784	0.953	1.796	1.784	0.909
Ca	0.633	0.625	0.621	0.637	0.641	0.954	0.959	0.002	0.002			0.002	0.002	0.002	0.732	0.002	0.003	0.847
Na	0.133	0.134	0.131	0.134	0.129	0.044	0.037								0.099			0.102
Ni	0.001	0.003	0.002	0.001	0.000	0.000	0.001	0.008	0.008	0.007	0.005	0.007	0.008	0.008	0.002	0.008	0.008	0.001
^{IV}Al	0.132	0.123	0.121	0.136	0.130	0.242	0.034								0.049			0.005
^{VI}Al	0.174	0.178	0.181	0.178	0.175	0.030	0.000								0.070			0.002
Fe^{3+}	0.057	0.045	0.032	0.045	0.037	0.114	0.033			0.024	0.027				0.012			0.034
Fe^{2+}	0.153	0.162	0.177	0.172	0.178	0.061	0.100			0.309	0.408				0.067			0.033
Mg#	79.8	80.2	80.0	78.8	79.1	80.6	86.5	92.4	92.3	69.7	60.7	90.7	90.4	90.9	92.4	90.7	90.1	93.1
Cr#	0.8	0.8	0.5	0.1	0.3	3.8	1.5			52.4	52.1				34.8			91.9

Footnote: C, coarse (>100μm); C-c, coarse-core; C-r, coarse-rim; F, fine (<100μm); F-MP, fine grain in melt pocket; F-Gt, fine grain in reaction rim of garnet; FeO and Fe, total Fe; Mg# = Mg/(Mg + Fe) $\times$ 100 atomic ratio; Cr# = Cr/(Cr + Al) $\times$ 100 atomic ratio.

grains and some display breakdown texture perhaps suggesting decompression process. Fine-grained olivines occasionally occur as inclusion within clinopyroxenes with spongy texture (Fig. 3h). Melt pocket is not found and rare minor mineral occur in the type 2 xenoliths.

4. Analytical method

Major element compositions of minerals were determined using Cameca SX50 at the Institute of Geology and Geophysics, Chinese Academy of Sciences. All analyses were performed with a beam of 15 keV and 20 nA and the precision is around 1.5%. The results are given in Table 2. Backscattered images (Fig. 4) were also obtained with Cameca SX50.

5. Mineral chemistry

5.1. Olivine

According the Fo (forsterite) content in olivine, Haoti xenoliths can be divided into type 1 with high Fo (>90) and type 2 with low Fo (⩽90). Overall, coarse-grained olivines have higher NiO contents than the fine-grained ones in both types (Table 2 and Fig. 5), whereas, CaO contents (generally >0.10 wt%) of fine-grained olivines are lightly higher than those (generally <0.10 wt%) in coarse-grained ones (Table 2). However, coarse-grained olivines in type 1 xenoliths have lower Fo than the fine-grained ones in the individual sample, which is on the contrary for that in type 2.

5.2. Clinopyroxene

Clinopyroxenes from the type 1 xenoliths are all endiopside with low Wo values (40–45), while those from the type 2 peridotites are diopside with high Wo values (>45) and clinopyroxene megacrysts plot within augite field (Fig. 6). Haoti clinopyroxenes have higher contents of Cr_2O_3 (0.92–6.87 wt%; Table 2), i.e., they are subordinate to chromium diopside (>0.5 wt%) as defined by Fan et al. (2005). The type 1 clinopyroxenes have lower Al_2O_3 + CaO and higher Mg# than the type 2 ones (Fig. 7a). Fine-grained clinopyroxenes have lower Al_2O_3 + CaO values than coarse-grained ones regardless of the types (Fig. 7a). Mg#s in clinopyroxene megacrysts

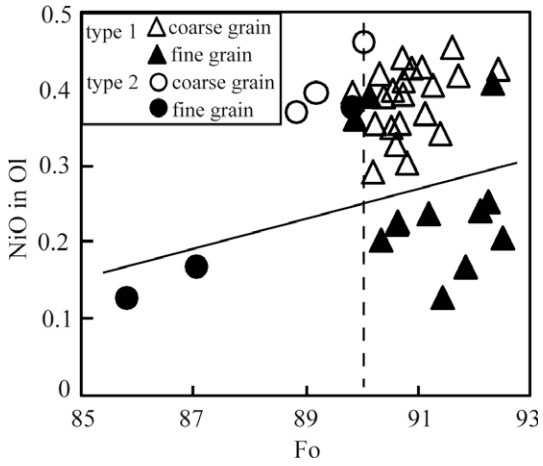

Fig. 5. Plot of Fo and NiO contents of olivine in Haoti peridotitic xenoliths. The dashed line is the boundary between the type 1 and type 2, and the bold line is the boundary between fine and coarse grains.

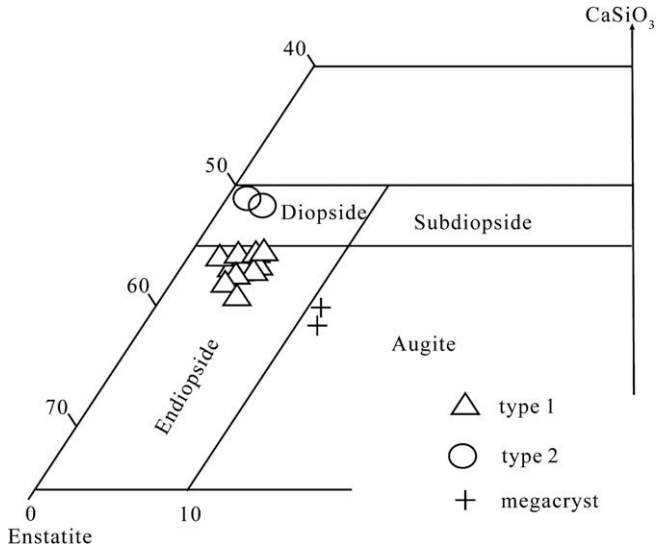

Fig. 6. Classification of clinopyroxene (Poldervaart and Hess, 1951) showing pretty different component of clinopyroxene from the type 1 and type 2 xenoliths and megacryst.

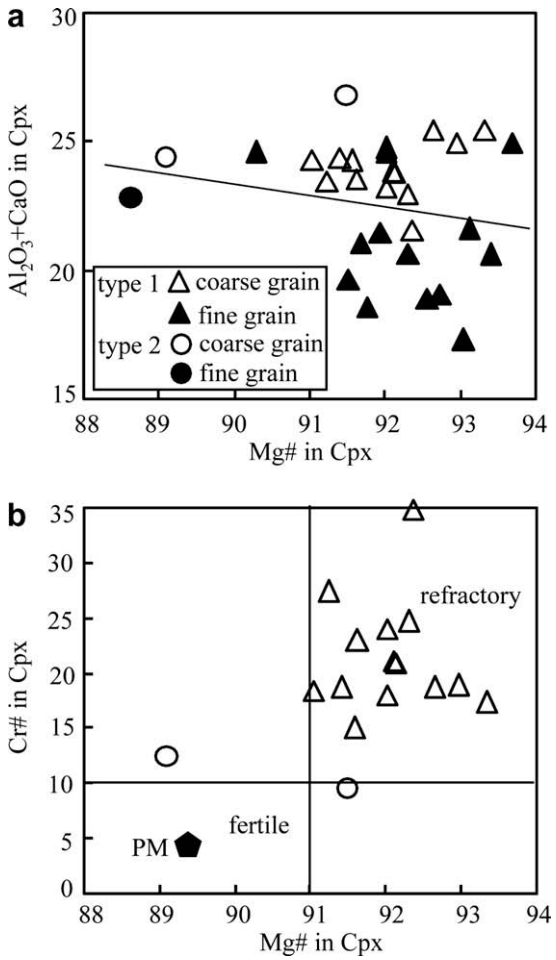

Fig. 7. Clinopyroxene composition in Haoti xenoliths. (a) Al_2O_3 + CaO and Mg# values in coarse and fine clinopyroxene grains, the line is the boundary between fine and coarse grains; (b) Plot of Mg# vs. Cr# in clinopyroxene. The refractory mantle quadrant is defined by Cr# ⩾ 10 and Mg# ⩾ 91 for Hebi clinopyroxenes (Zheng et al., 2001). PM, Primitive Mantle (McDonough and Sun, 1995).

are remarkably lower (78.8–80.2; Table 2) than that in peridotites. All clinopyroxenes from the type 1 xenoliths are plotted in the refractory mantle field, defined by the Cr# (⩾10) and Mg# (⩾91) from the Hebi in the North China Craton, which was interpreted to represent old refractory mantle (Zheng et al., 2001), while type 2 clinopyroxenes show fertile feature (Fig. 7b).

5.3. Orthopyroxene

Orthopyroxenes in Haoti peridotites dominantly occur as coarse grains, only two samples contain fine grains and hence it is difficult to obtain compositional comparisons for different grain sizes. Some orthopyroxenes of sample HT-16 have porphyroclastic texture, in that fine-grained olivines and clinopyroxenes surrounding the orthopyroxenes (Fig. 4d). The porphyroclastic orthopyroxene from HT-16 has distinctive compositions from those in other samples, reflected by higher En contents (90.7–90.9) and Mg# (92.2–92.5), and lower Al_2O_3 contents (1.52–1.56 wt%; Table 2). The presence of this unusually low-Al and high-Mg# orthopyroxene is a typical characteristic of depleted xenoliths (Cvetkovic et al., 2007). In comparison, orthopyroxenes of xenoliths from off-cratonic settings generally contain 3.0–6.0 wt% Al_2O_3 (Pearson et al., 2003).

5.4. Spinel and chromite

Spinels from the type 1 xenoliths are generally fine grains and have high Cr_2O_3 (30.4–49.1 wt%) and low Al_2O_3 (21.0–36.6 wt%) contents, thus they are classified as Cr-spinel and fall within or close to the range of cratonic chromium spinels (Cr# = 40–91; Zhou et al., 1994; Griffin et al., 1998; Zheng, 1999). The spinels from the type 2 xenoliths occur as coarse grains and are subordinate to Al-spinel according to their low Cr_2O_3 (5.56–18.28 wt%) and high Al_2O_3 (40.5–62.0 wt%) contents. Some of the type 2 spinels with breakdown texture have slightly higher Cr# in the core than in the rim (Table 2). Fine-grained chromites are found in the microcracks between main minerals and their compositions are shown in Table 2.

5.5. Garnet

One garnet lherzolite (HT-32) was collected in this study, in which five phases (Ol + Cpx + Opx + Gt + Sp) coexist (Fig. 4g and h). The interstitial garnet shows clear reaction rim suggesting interaction with olivine related to decompression. Secondary minerals in garnet reaction rim are mainly fine-grained clinopyroxene (Mg#, 88.6; Cr#, 6.4), orthopyroxene (Mg#, 89.1), spinel (Cr#, 9.8) and olivine (Mg#, 89.9), which show low Mg# and/or Cr# compared with primary minerals. This shows disequilibrated five coexistent phases and transition from garnet to spinel stability field.

5.6. Amphibole, phlogopite, feldspar, calcite and ilmenite

Amphiboles presented in the type 1 xenoliths are usually related with clinopyroxenes (Fig. 4c). Compared with the amphiboles from the Hebi peridotites (Zheng et al., 2001), Haoti amphiboles are rich in SiO_2, NiO, Na_2O and poor in Al_2O_3, Cr_2O_3. Phlogopites in the cracks of pyroxenes or olivines have higher SiO_2, Na_2O and lower TiO_2, Al_2O_3, K_2O, MgO, CaO contents than phlogopite phenocrysts (Yu et al., 2000). Feldspars occur as vein in both types (Fig. 4e and f) and are either orthoclase or albite in composition. Calcites and ilmenites are also found in these peridotitic xenoliths and occur as veins and as discrete fine grain, respectively.

6. Discussion

6.1. Pressure and temperature estimation

In many geothermometers and geobarometers, Fe^{3+}, Fe^{2+}, Al^{IV} and Al^{VI} of minerals are significant parameters (e.g., Wood and Banno, 1973; Wells, 1977; Sachtleben and Seck, 1981; Witt and Seck, 1991; Brey and Kohler, 1990; Kohler and Brey, 1990; O'Reilly and Griffin, 1995; Woodland et al., 2006), although some researchers suggested that all Fe be taken as Fe^{2+} for both clinopyroxene and garnet using garnet–clinopyroxene thermometer (e.g., Carswell and Gibb, 1987). In this study, Fe^{3+} and Fe^{2+} have been calculated for two pyroxenes, garnet and spinel from charge balance based on six, twelve and four oxygens, respectively. Structural formulae for spinel were estimated on the general stoechiometry: (Al, Cr, Fe^{3+}) (Mg, Fe^{2+}, Mn, Zn) O_4. The distributions of Al in pyroxene were estimated according to $Al^{IV} = 2 - Si$ and $Al^{VI} = Al - Al^{IV}$.

Equilibration temperatures for coarse grains of the Haoti xenoliths have been estimated using geothermometers of Wells (1977), Wood and Banno (1973), Sachtleben and Seck (1981) and Witt and Seck (1991) and given in Table 3. T(W) two-pyroxene thermometer, T(SS) spinel-orthopyroxene thermometer and T(WS2) spinel-orthopyroxene thermometer generally show good agreement for most samples. The equilibration temperatures of the type 1 xenoliths are in a range from 1106 to 1187 °C using two-pyroxene thermometer of Wood and Banno (1973) and those of the type 2 xenoliths range from 1015 to 1103 °C. Coarse-grained garnet–orthopyroxene mineral assemblage in a garnet lherzolite (HT-32) yields a temperature–pressure estimation of 1071 °C and 23 kbar (Brey and Kohler, 1990), corresponding to a depth of 74 km (Fig. 10), according to the empirical formula D (depth) = 4.02 + 3.03P (pressure) (Lallemant et al., 1980). Pressures of spinel lherzolite were estimated by Ca contents in olivine (Kohler and Brey, 1990). Type 1 spinel lherzolites show relatively high pressure (>21 kbar) and some give higher values than garnet peridotite which is perhaps related to the precision of these geobarometers, whereas type 2 xenoliths have lower than 19 kbar pressure (Table 3).

6.2. Nature of the lithospheric mantle beneath the western Qinling

It has been recognized with experiments (e.g., Jaques and Green, 1980) and natural samples (e.g., Arai, 1994) that Cr# of spinel and Fo content in olivine progressively increase with enlargement of the extent of melt extraction. The Mg# and Cr# of

Table 3
Estimations of temperature (°C) and pressure (kbar) for Haoti xenoliths

Sample	T (W)	T (WB)	T (SS)	T (WS1)	T (WS2)	P (KB)	P (BK)
Type 1							
HT-08	1108	1187	1131	964	1070	24.9	
HT-15	1061	1153	1139	913	1082	21.1	
HT-23	905	1018					
HT-32	1071	1150					23
HT-25	1008	1106	1012	951	1032	21.8	
HT-33	1097	1175	1140	1107	1098	24.3	
HT-46	1089	1174	1119	1028	1090	24.3	
HT-43	1103	1186					
HT-16	1030	1133				22.8	
Type 2							
HT-04	907	1015	1006	938	989	19.0	
HT-24	1022	1103	908	783	971	18.5	

Note: T (W), Wells (1977), two-pyroxene thermometer; T (WB), Wood and Banno (1973), two-pyroxene thermometer; T (SS), Sachtleben and Seck (1981), Sp-Opx thermometer; T (WS1) and T (WS2), Witt and Seck (1991), Cr-Al-Opx thermometer and Sp-Opx thermometer; P (KB), Kohler and Brey (1990), Ca-in-Ol geobarometer; P (BK), Brey and Kohler (1990), Opx-Grt barometer.

clinopyroxene are also distinguished as sensitive indicators of the extent to refractory of mantle peridotites (Frey and Prinz, 1978; Henry and Thomas, 1984; Preb et al., 1986). Therefore, Cr# of spinel, Fo content in olivine and Mg# and Cr# of clinopyroxene are generally used to infer the degree of depletion in mantle peridotite. Cr#s of spinels from Haoti type 1 xenoliths range from 36 to 67 and Fo contents in olivines are in the variation of 90–92.5, while Mg#s and Cr#s of clinopyroxenes are in range of 91–94 and 15–35, respectively, and plot within the refractory field in Fig. 7b. This evidence is consistent with the above partial melting relationship. However, the type 2 peridotites have relatively low corresponding indicators, implying a fertile characteristic.

Boyd (1989) have used the major element compositions of mantle-derived xenoliths and oceanic peridotites to demonstrate a marked differences of producing subcontinental lithospheric mantle between Archean, Proterozoic and Phanerozoic time in the plot of olivine modal percentage against Fo content in olivine (Fig. 8). Haoti type 1 peridotites basically plot near even within Proterozoic field and slightly show an oceanic peridotite trend (melting trend), whereas the type 2 peridotites are closely related to Phanerozoic lherzolite field (Fig. 8). Furthermore, Haoti type 1 peridotites have the similar refractory characteristic to Hebi peridotite representing old refractory mantle and the type 2 xenoliths plot outside of the field (Fig. 7b). In addition, the trace element and isotopic compositions of the host rock revealed that the western Qinling kamafugite has OIB-like characteristics (Yu, 1994; Yu et al., 2000, 2004, 2005). Mo et al. (2006) compiled the data of postcollisional volcanic rocks from the Tibetan Plateau and its adjacent regions and suggested that Tethyan oceanic component should be involved into the Cenozoic magmatic activities. Therefore, we speculate that, although no chronological study on mantle xenoliths, Haoti type 1 xenoliths are likely to represent old refractory lithospheric mantle perhaps involving Tethyan oceanic component and that the type 2 xenoliths possibly is the representation of newly-accreted lithospheric mantle.

6.3. Partial melting, recrystallization and metasomatism

Al_2O_3 and CaO contents in peridotite can mirror the degree of basaltic component extraction, which can only be used in the case that no later metasomatism event overlapped after the partial melting process, because melt/fluid especially Ca-rich component can easily modify their records. However, residual signatures are largely preserved in depletion indicators such as Cr# of spinel, Fo content in olivine and Mg#, Cr# and heavy rare earth element concentrations in clinopyroxenes, because they are less sensitive to the effects of subsequent metamorphism and metasomatism. As shown above, these indicators as well as the petrological features such as melt pocket and low Al_2O_3 and high Mg# porphyroclastic orthopyroxene record the partial melting event in the lithospheric mantle beneath the western Qinling. The type 1 xenoliths have relatively higher Cr# of spinel but lower Na_2O content in clinopyroxene than the type 2, thus, Fig. 9 shows increasing partial melting trend from the type 2 peridotites to the type 1. The type 2 peridotites underwent low, less than 5% at most, degree of partial melting, whereas the type 1 xenoliths experienced high, more than 10%, degree of partial melting, which are consistent with the fertile and refractory compositions, respectively. P–T estimations indicate the fertile type 2 xenoliths is located at shallower part of lithospheric mantle than the refractory type 1, in other words, the degree of partial melting become higher with increasing depth. Therefore, the partial melting is not decompressional melting related to decompression event which will be discussed below.

Melt pockets formed during partial melting generally because of lack of time to permit migration and principally contain glass component (Dawson, 2002). In the case of the Haoti xenoliths, some melt pockets closed within their precursor are likely to be in situ melting and no migration in late-stage. The absence of glass

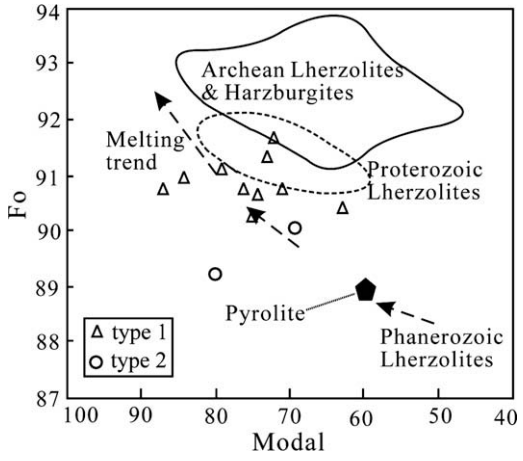

Fig. 8. Modal % of olivine vs. Fo in coarse-grained olivine from Haoti peridotitic xenoliths. Oceanic trend from Boyd (1989); Archean, Proterozoic and Phanerozoic fields are from Griffin et al. (1999).

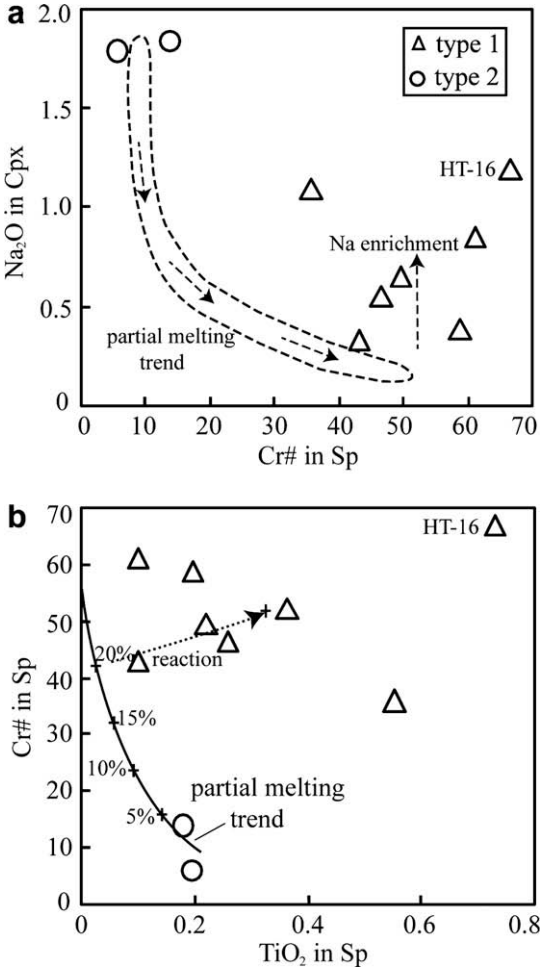

Fig. 9. Cr# of spinel vs. Na_2O of clinopyroxene (a) and TiO_2 of spinel (b) of Haoti peridotitic xenoliths. The higher Na_2O and TiO_2 in clinopyroxene and spinel from the type 1 xenoliths imply melt/rock interaction after high degree of partial melting (>10%), whereas the compositions of clinopyroxene and spinel from type 2 peridotites reveal low degree melting (<5%). Partial melting trend and parameters used here are as same as the reference in Xu et al. (2003).

in melt pockets implies that the length of time between the formation of the melt pockets and their subsequent quenching must have been so long that recrystallization occurred. Ambient minerals of the melt pockets are mainly olivine, clinopyroxene and orthopyroxene, but within melt pockets, the minerals are just limited to fine-grained olivine and clinopyroxene and the former is somewhat more than the latter. Therefore, recrystallized olivines and clinopyroxenes possessing higher Mg# than coarse-grained ones can be easily understood and low NiO contents can be interpreted as the dilution of NiO in the melt. Besides, recrystallized clinopyroxenes could not take possession of all the CaO dissolved from their precursor, additional CaO had to enter olivines resulting in their higher CaO contents. Fine-grained minerals in the type 2 xenoliths mostly occur as inclusions and possibly crystallized a little bit earlier than coarse-grained ones implying compositional heterogeneity of newly-accreted lithospheric mantle.

Actually, the type 1 xenoliths (Fig. 9) apparently shift from partial melting trend to Na enrichment or reaction trend evidenced by higher Na_2O of clinopyroxenes and higher TiO_2 of spinels. This feature suggests metasomatism happened following the partial melting. Particularly, HT-16 of the type 1 xenoliths has the highest Na_2O contents of clinopyroxenes and highest TiO_2 contents of spinels, which is consistent with the presences of phlogopite and amphibole, a strong signature of modal metasomatism.

Peridotite–melt/fluid interaction in orogenic peridotites (Bodinier et al., 1990; Smith et al., 1999) characterized by dissolution of orthopyroxene and precipitation of olivine, sometimes in accompany with the generation of clinopyroxenite veins and dunites is described as: orthopyroxene + melt 1 = olivine + SiO_2 (melt 2) (+clinopyroxene) (Zhang, 2005a,b; Zhang et al., 2007a). Experiments on peridotite xenoliths indicate that clinopyroxenes can be caused by partial dissolution of the minerals in reaction with melt at temperature below 1260 °C (Tsuchiyama, 1986; Shaw et al., 2006). Haoti peridotitic xenoliths have lower modal proportions of orthopyroxene but higher olivine. All the equilibration temperatures for Haoti xenoliths range from 1000 °C to 1200 °C (Table 3). In addition, some clinopyroxenes and spinels have character of sieved texture. These lines of features further indicate the interaction between peridotite and melt. The melt is apparently rich in Na and Ti shown in Fig. 9 and perhaps rich in Ca according to the presence of calcite in Haoti xenoliths.

The western Qinling kamafugites show ocean island basalt (OIB)-restricted isotopic ranges including $^{87}Sr/^{86}Sr$ values ranging from 0.70383 to 0.70623, $^{143}Nd/^{144}Nd$ values ranging from 0.51277 to 0.51292 and $^{206}Pb/^{204}Pb$ and $^{207}Pb/^{204}Pb$ values in range of 18.418–18.928 and 15.476–15.589, respectively (Table 4). The kamafugites and its coexisting carbonatites display OIB-like rare earth element and (non-depleted or even slightly enriched) HFSE patterns (Yu et al., 2004; Mo et al., 2006). Based on the generation of primitive kamafugite with Sr, Nd, and Pb isotopic ranges and OIB-like trace-element characteristics, Yu et al. (2004) and Mo et al. (2006) proposed that plume-like asthenospheric upwelling existed beneath the western Qinling. The Cenozoic volcanic rocks around Tibetan Plateau, including the western Qinling, have both OIB-like and intercontinental volcanic characteristics, reflecting the presence of a residual recycling paleo-oceanic crust in mantle (Deng, 1996; Mo et al., 2006). Seismic tomography demonstrated there was a large rock-massif in 670 km depth (Liu et al., 1989). These observations reveal the existence of Paleo-Tethyan oceanic crust, which might make some contributions to the source of the melt.

Table 4
Sr–Nd–Pb isotope compositions of the Western Qinling kamafugites (Yu et al., 2004; Mo et al., 2006)

Sample	$^{87}Sr/^{86}Sr$	$^{143}Nd/^{144}Nd$	$^{206}Pb/^{204}Pb$	$^{207}Pb/^{204}Pb$
2003	0.70383	0.51285	18.634	15.525
2004	0.70443	0.51289	18.928	15.557
2008	0.70623	0.51292	18.624	15.539
2009	0.70450	0.51283	18.643	15.574
2011	0.70429	0.51289	18.625	15.552
2014	0.70540	0.51278	18.886	15.589
2104	0.70403	0.51289	18.728	15.573
2108	0.70516	0.51279	18.666	15.555
2112	0.70401	0.51286	18.524	15.482
8752	0.70425	0.51288	18.418	15.544
8628	0.70438	0.51279	18.625	15.514
8617	0.70412	0.51278	18.455	15.551
9113	0.70525	0.51291	18.589	15.490
9118	0.70419	0.51277	18.617	15.476
9126	0.70434	0.51277	18.571	15.523

6.4. Deformation, decompression and tectonic implication

In the 1970s, some geologists began to study the textures, microstructures and deformation processes of ultra-mafic xenoliths and discovered "deformed peridotitic xenoliths" (Mercier and Nicolas, 1975; Basu, 1977; Coisy and Nicolas, 1978). Three textural types, including porphyroclastic, fine-grained equigranular, and mylonitized or cataclastic textures, were recognized in these deformed peridotite xenoliths (Harte, 1977). Textural variations in deformed peridotites had previously been interpreted as the result of large-scale asthenospheric mantle diapirism (Nicolas et al., 1987; Witt and Seck, 1987). However, some studies suggested that small-scale lithospheric shearing could be a better explanation (e.g., Downes, 1990; Bjerg et al., 2005). So far, many authors (e.g., Coisy and Nicolas, 1978; Ross, 1980; Nicolas et al., 1987; Witt and Seck, 1987; Downes, 1990; Bjerg et al., 2005) have reached the agreement that the occurrence of abundant deformed peridotites is evidence of diapirism of active upwelling mantle.

Textures of Haoti peridotites, such as porphyroclastic feature and mineral elongation (Fig. 3a–d) indicate that the Haoti peridotites underwent strong deformations. During deformation process, coarse-grained minerals were not only elongated, but also broken down into pieces, resulting in some fine grains present around coarse grains and having similar compositions (Figs. 5 and 7a). The deformation is always related to the mantle metasomatism such as the presence of pervasive amphibole (Nicolas et al., 1987) and the geochemical enrichment in clinopyroxenes with high ε_{Sr} and low ε_{Nd} values and in light rare earth elements (e.g., Downes, 1990). In the Haoti xenoliths, some cracks developing within clinopyroxenes vanish in the feldspar veins and some cross them (Fig. 4e and f). Combination with the presence of pervasive amphibole, it is suggested deformation and metasomatism likely happened synchronously.

P–T estimations of peridotitic xenoliths revealed that the main constituents of lithospheric mantle beneath the western Qinling are spinel lherzolite and garnet lherzolite whose boundary (transition zone) is located at the depth of around 78 km, and that the lower geothermal flow beneath the western Qinling than that in eastern China (Fig. 10) where thick lithospheric mantle has been significantly thinned (e.g., Menzies et al., 1993; Fan et al., 2000; Zhang, 2005a,b; Zhang et al., 2007a, 2008). Thick lithosphere beneath the western Qinling (at least 100 km) can be interpreted as two possibilities that (1) no or just small-scale thinning relative to eastern China lithosphere, and (2) lithospheric thickening or accretion. There is not a plenty of studies to respond to the possibility 1 (Su et al., 2007), however, lithospheric thickening in Tibetan Plateau and its adjacent regions has been strongly clarified (e.g., Houseman and England, 1993; Jiang et al., 2006; Zhang et al., 2007b). Taking into account the tectonic relationship of Tibetan Plateau and western Qinling, possibility 2 should be more suitable.

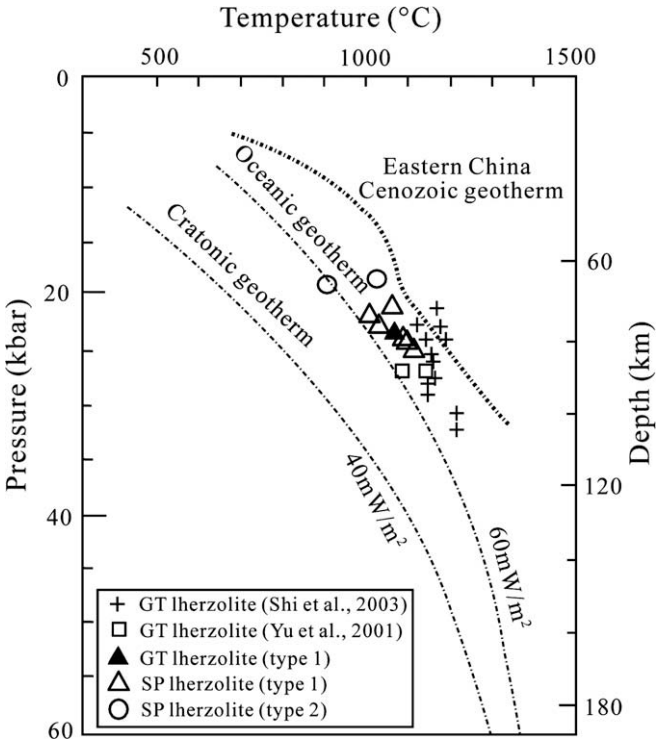

Fig. 10. P–T estimates for Haoti spinel and garnet peridotites including previous work and this study. Typical cratonic and oceanic geotherms from Menzies and Chazot (1995); Eastern China Cenozoic geothermal from Xu et al. (1995) and Su et al. (2007).

On the other hand, breakdown textures of garnet from the type 1 xenoliths (Fig. 3f; Fig. 4g and h) and spinel from the type 2 xenoliths, especially spongy texture of clinopyroxene from the type 2 (Fig. 3g and h), have been observed, which implies a decompression event. The decompression must be a latest event happed in the lithospheric mantle beneath the western Qinling because its signature is recorded in both type xenoliths. It is also a response to the latest extensive tectonic environment, which induced Cenozoic fault-bounded basins such as Tianshui-Lixian fault basin and well-developed deep faults along NW–SE direction in the region (Zhang et al., 2001a)

7. Conclusions

(1) The Haoti xenoliths have two distinctive populations, type 1 and type 2 based on their mineral compositions. The compositions of fine-grained minerals in these xenoliths are apparently different from those of coarse-grained ones.
(2) The type 1 xenoliths are characterized by the depleted, metasomatic and deformed characteristics, and may represent the old refractory lithospheric mantle. In contrast, the type 2 peridotites have fertile feature and may represent the newly-accreted lithospheric mantle.
(3) The lithospheric mantle beneath the western Qinling was composed of spinel and garnet lherzolite with the thickness of at least 100 km and underwent partial melting, recrystallization, deformation and metasomatism due to the asthenospheric upwelling and the latest decompression responding to the Cenozoic extensive tectonic environment. These processes are perhaps closely related to the formation and evolution of Tibetan Plateau caused by the India-Asian collision.

Acknowledgments

This research was financially supported by the Knowledge Innovation Program of the Chinese Academy of Sciences (Grant KZCX2-YW-103), the National Science Foundation of China (Grants 40534022, 90714008, and 40721062) and the grant from the Univeristy of Hong Kong. The authors would like to extend special thanks to Q. Mao and Y.G. Ma for their assistance in major elements analyses at the State Key Laboratory of Lithospheric Evolution of the IGG, and thank Y.J. Tang and W.H. Zhang for their thoughtful discussion. Patrick Sakyi is also appreciated for improving the original manuscript.

References

Arai, S., 1994. Characterization of spinel peridotites by olivine-spinel compositional relationships: review and interpretation. Chemical Geology 113, 191–204.
Basu, A.R., 1977. Textures, microstructures and deformation of ultramafic xenoliths from San Qsuintin, Baja California. Tectonophysics 43, 213–246.
Bjerg, E.A., Ntaflos, T., Kurat, G., Dobosi, G., Labudıa, C.H., 2005. The upper mantle beneath Patagonia, Argentina, documented by xenoliths from alkali basalts. Journal of South America Earth Science 18, 125–145.
Bodinier, J.L., Vasseu, R.G., Vernieres, J., Dupuy, J., Fabries, J., 1990. Mechanisms of mantle metasomatism: geochemical evidence from the lherz orogenic peridotite. Journal of Petrology 31, 597–628.
Boyd, F.R., 1989. Composition and distinction between oceanic and cratonic lithosphere. Earth and Planetary Science Letters 96, 15–26.
Boyd, F.R., Pokhilenko, N.P., Pearson, D.G., Mertzman, S.A., Sobolev, N.V., Finger, L.W., 1997. Composition of the Siberian cratonic mantle: evidence from Udachnaya peridotite xenoliths. Contributions to Mineralogy and Petrology 128, 228–246.
Brey, G.P., Kohler, T., 1990. Geothermobarometry in four-phase lherzolites II, new thermobarometers and practical assessment of existing thermobarometers. Journal of Petrology 31, 1353–1378.
Carswell, D.A., Gibb, F.G.F., 1987. Evaluation of mineral thermometers and barometers applicable to garnet lherzolite assemblages. Contributions to Mineralogy and Petrology 95, 499–511.
Chen, Z.H., Lu, S.N., Li, H.K., Li, H.M., Xiang, Z.Q., Zhou, H.Y., Song, B., 2006. Constraining the role of the Qinling orogen in the assembly and break-up of Rodinia: Tectonic implications for Neoproterozoic granite occurrences. Journal of Asian Earth Sciences 28, 99–115.
Coisy, P., Nicolas, A., 1978. Regional structure and geodynamics of the upper mantle beneath the Massif Central. Nature 274, 429–432.
Cvetkovic, V., Downes, H., Prelevic, D., Lazarov, M., ResimicSaric, K., 2007. Geodynamic significance of ultramafic xenoliths from Eastern Serbia: Relics of sub-arc oceanic mantle? Geodynamics 43, 504–527.
Dawson, J.B., 2002. Metasomatism and partial melting in upper-mantle peridotite xenoliths from the Lashaine Volcano, Northern Tanzania. Journal of Petrology 43, 1749–1777.
Deng, W.M., 1996. Basic–ultrabasic and volcanic rocks in Chagbu–Shuanghu area of northern Xizang (Tibet). Science in China (D) 39, 359–368.
Deng, W.M., 2003. Cenozoic volcanic activity and its geotectonic background in west China – formative excitation mechanism of volcanic rocks in Qinghai–Xizang and adjacent districts. Earth Science Frontiers 10, 471–478. in Chinese with English abstract.
D'Orazio, M., Innocenti, F., Tonarini, S., Doglioni, C., 2007. Carbonatites in a subduction system: the Pleistocene alvikites from Mt. Vulture (southern Italy). Lithos 98, 313–334.
Downes, H., 1990. Shear zones in the upper mantle – relation between geochemical enrichment and deformation in mantle peridotites. Geology 18, 374–377.
Fan, W.M., Zhang, H.F., Baker, J., Jarvis, K.E., Mason, P.R.D., Menzies, M.A., 2000. On and off the North China Craton: where is the Archean Keel? Journal of Petrology 41, 933–950.
Fan, Q.C., Zhang, H.F., Sui, J.L., Zhai, M.G., Sun, Q., Li, N., 2005. Magma intrusion and current component of crust–mantle boundary in Hannuoba: evidence from petrology of xenoliths and geochemistry. Science in China (D) 35, 1–4.
Foley, S.F., Venturelli, G., Green, D.H., Toscani, L., 1987. The ultrapotassic rocks: characteristics, classification and constraints for petrogenetic models. Earth Science Reviews 24, 81–134.
Frey, F.A., Prinz, M., 1978. Ultramafic inclusions from San Carlos, Arizona: petrologic and geochemical data bearing on their petrogenesis. Earth and Planetary Science Letters 38, 129–176.
Gao, S., Zhang, B.R., Wang, D.P., Ouyang, J.P., Xie, Q.L., 1996. Geochemical evidence for the Proterozoic tectonic evolution of the Qinling Orogenic Belt and its adjacent margins of the North China and Yangtze cratons. Precambrian Research 80, 23–48.
Griffin, W.L., Zhang, A.D., O'Reilly, S.Y., Ryan, C.G., 1998. Phanerozoic evolution of the lithosphere beneath the Sino-Korean craton. In: Flower, M., Chung, S.L., Lo, C.H., Lee, Y.Y. (Eds.), Mantle Dynamics and Plate Interactions in East Asia, Geodynamic Series, vol. 27. American Geophysical Union, Washington DC, pp. 107–126.

Griffin, W.L., O'Reilly, S.Y., Ryan, C.G., 1999. The composition and origin of sub-continental lithospheric mantle. In: Fei, Y., Bertka, C., Mysen, B.O. (Eds.), Mantle Petrology: Field Observations and High-Pressure Experimentation. The Geochemical Society. Stony Brook, pp. 13–45.

Harte, B., 1977. Rock nomenclature with particular reference to deformation and recrystallization textures in olivine bearing xenoliths. The Journal of Geology 85, 279–288.

Henry, J.B.D., Thomas, B., 1984. Chromian spinel as a petrogenetic indicator in abyssal and alpine-type peridotites and spatially associated lavas. Contributions to Mineralogy and Petrology 86, 54–76.

Houseman, G., England, C., 1993. Crustal thickening versus lateral expulsion in the India-Asian continental collision. Journal of Geophysical Research 98, 12233–12249.

Kohler, T.P., Brey, G.P., 1990. Calcium exchange between olivine and clinopyroxene calibrated as a geobarometer for natural peridotites from 2 to 60 kbar with applications. Geochimica et Cosmochimica Acta 54, 2375–2388.

Jaques, A.L., Green, D.H., 1980. Anhydrous melting of peridotite at 0–15 kb pressure and the genesis of tholeiitic basaltic magma. Contributions to Mineralogy and Petrology 73, 287–310.

Jiang, M., Galvé, A., Hirn, A., Voogd, B., Laigle, M., Su, H.P., Diaz, J., Lépine, J.C., Wang, Y.X., 2006. Crustal thickening and variations in architecture from the Qaidam basin to the Qang Tang (North-Central Tibetan Plateau) from wide-angle reflection seismology. Tectonophysics 412, 121–140.

Lallemant, A., Mercier, H.G., Carter, J.C., Ross, J.V., 1980. Rheology of upper mantle: inferences from peridotite xenoliths. Tectonophysics 70, 85–113.

Liu, F.T., Qu, K.X., Wu, H., Li, Q., Liu, J.H., Hu, G., 1989. Seismic tomography of the Chinese continent and adjacent region. Acta Geophysica Sinica 32, 281–291. in Chinese with English abstract.

Liu, S.J., 1996. Giant crystals occurred the tertiary ultramafic rocks and their forming conditions in Haoti, Dangchang county. Acta Geologica GanSu 2, 65–72. in Chinese with English abstract.

Lloyd, F.E., Edgar, A.D., Ragnarsdottir, K.V., 1996. LREE distribution in pervoskite, apatite and titanite from South West Ugandan xenoliths and kamafugite lavas. Mineralogy and Petrology 57, 205–228.

McDonough, W.F., Sun, S.S., 1995. The composition of the Earth. Chemical Geology 120, 223–253.

Menzies, M.A., Chazot, G., 1995. Fluid processes in diamond to spinel facies shallow mantle. Journal of Geodynamics 20, 387–415.

Menzies, M.A., Fan W.M., Zhang, M., 1993. Paleozoic and Cenozoic lithoprobes and the loss of >120 km of Archean lithosphere, Sino-Korean craton, China. In: Prichard, H.M., Alabaster, T., Harris, N.B.W., Neary, C.R. (Eds.), Magmatic processes and plate tectonics 76, pp. 71–81.

Mercier, J.C.C., Nicolas, A., 1975. Textures and fabrics of upper mantle peridotites as illustrated by xenoliths from basalts. Journal of Petrology 16, 454–487.

Mo, X.X., Zhao, Z.D., Deng, J.F., Flower, M., Yu, X.H., Luo, Z.H., Li, Y.G., Zhou, S., Dong, G.C., Zhu, D.C., Wang, L.L., 2006. Petrology and geochemistry of postcollisional volcanic rocks from the Tibetan plateau: implications for lithosphere heterogeneity and collision-induced asthenospheric mantle flow. Special paper, Postcollisional Tectonics and Magmatism in the Mediterranean Region and Asia 409, pp. 507–530.

Nicolas, A., Lucazeau, F., Bayer, R., 1987. Peridotite xenoliths in massif central basalts: textural and geophysical evidence for asthenospheric diapirism. In: Nixon, P.H. (Ed.), Mantle Xenoliths. Wiley and Sons, Chichester, England, pp. 461–474.

O'Reilly, S.Y., Griffin, W.L., 1995. Trace-element partitioning between garnet and clinopyroxene in mantle-derived pyroxenites and eclogites: P–T–X controls. Chemical Geology 121, 105–130.

Pearson, D.G., Canil, D., Shirey, S.B., 2003. Mantle samples included in volcanic rocks: xenoliths and diamonds. In: Holland, H.D., Turekian, K.K. (Eds.), Treatise on Geochemistry, pp. 171–275.

Poldervaart, A., Hess, H.H., 1951. Pyroxene in the crystallization of basaltic magma. The Journal of Geology 59, 472–489.

Preb, S., Witt, G., Seck, H.A., Eonov, D., Kovalenko, V.I., 1986. Spinel peridotite xenoliths from the Tariat Depression, Mongolia: major element chemistry and mineralogy of a primitive mantle xenolith suite. Geochimica et Cosmochimica Acta 50, 2587–2599.

Ross, J.V., 1980. The mantle and rheology of the Cordilleran upper mantle of British Columbia: inferences from peridotite xenoliths. Tectonophysics 100, 321–357.

Sachtleben, T.H., Seck, H.A., 1981. Chemical control of Al-solubility in orthopyroxene and its implications on pyroxene geothermometry. Contributions to Mineralogy and Petrology 78, 157–165.

Schmidberger, S.S., Francis, D., 1999. Nature of the mantle roots beneath the North American craton: mantle xenolith evidence from Somerset Island kimberlites. Lithos 48, 195–216.

Sgarbi, P.B.A., Heaman, L.M., Gaspar, J.C., 2004. U–Pb perovskite ages for brazilian kamafugitic rocks: further support for a temporal link to a mantle plume hotspot track. Journal of South American Earth Sciences 16, 715–724.

Shaw, C.S.J., Heidelbach, F., Dingwell, D.B., 2006. The origin of reaction textures in mantle peridotite xenoliths from Sal Island, Cape Verde: the case for "metasomatism" by the host lava. Contributions to Mineralogy and Petrology 151, 681–697.

Shi, L.B., Lin, C.Y., Chen, X.D., 2003. Composition, thermal structures and rheology of the upper mantle inferred from mantle xenoliths from Haoti, Dangchang, Gansu Province, western China. Seismology and Geology 4, 525–542. in Chinese with English abstract.

Smith, D., Alexis, R.J.C., Mertzman, S.A., 1999. Water–rock interactions, orthopyroxene growth, and Si-enrichment in the mantle: evidence in xenoliths from the Colorado Plateau, southwestern United States. Earth and Planetary Science Letters 165, 45–54.

Su, B.X., Chen, Y.L., Liu, F., Wang, Q.Y., Zhang, H.F., Lan, Z.W., 2006a. Geochemical characteristics and significance of Triassic sandstones of Songpan–Ganze block. Acta Petrologica Sinica 22, 961–970. in Chinese with English abstract.

Su, B.X., Zhang, H.F., Xiao, Y., Zhao, X.M., 2006b. Characteristics and geological significance of olivine xenocrysts in Cenozoic volcanic rocks from western Qinling. Progress in Natural Science 16, 1300–1306.

Su, B.X., Zhang, H.F., Wang, Q.Y., Sun, H., Xiao, Y., Ying, J.F., 2007. Spinel–garnet phase transition zone of Cenozoic lithospheric mantle beneath the eastern China and western Qiling and its T–P conditions. Acta Petrologica Sinica 23, 1313–1320. in Chinese with English abstract.

Tommasi, A., Vauchez, A., Ionov, D.A., 2008. Deformation, static recrystallization, and reactive melt transport in shallow subcontinental mantle xenoliths (Tok Cenozoic volcanic field, SE Siberia). Earth and Planetary Science Letters. doi:10.1016/j.epsl.2008.04.020.

Tsuchiyama, A., 1986. Melting and dissolution kinetics: application to partial melting and dissolution of xenoliths. Journal of Geophysics Research 91, 9395–9406.

Wells, P.R.A., 1977. Pyroxene thermometry in simple and complex systems. Contributions to Mineralogy and Petrology 62, 129–139.

Witt, G.E., Seck, H.A., 1987. Temperature history of sheared mantle xenoliths from the West Eifel, West Germany: evidence for mantle diaprism beneath the Rhenish Massif. Journal of Petrology 28, 475–493.

Witt, G.E., Seck, H.A., 1991. Solubility of Ca and Al in orthopyroxene from spinel peridotite: An improved version of an emoirical geothermometer. Contributions to Mineralogy and Petrology 106, 431–439.

Wood, B.J., Banno, S., 1973. Garnet–orthopyroxene relationships in simple and complex systems. Contributions to Mineralogy and Petrology 42, 109–124.

Woodland, A.B., Kornprobst, J., Tabit, A., 2006. Ferric iron in orogenic lherzolite massifs and controls of oxygen fugacity in the upper mantle. Lithos 89, 222–241.

Xu, Y.G., Lin, C.Y., Shi, L.B., Mercier, J.C.C., Ross, J.V., 1995. Upper mantle geotherm for eastern China and its geological implications. Science in China (B) 28, 525–542. in Chinese.

Xu, Y.G., Menzies, M.A., Thirlwall, M.F., Huang, X.L., Liu, Y., Chen, X.M., 2003. "Reactive" harzburgites from Huinan, NE China: products of the lithosphere–asthenosphere interaction during lithospheric thinning? Geochimica et Cosmochimica Acta 67, 487–505.

Yu, X.H., 1991. Mantle xenoliths and megacrysts in ultramafic lamprophyres in Haoti, Gansu Province. Geological Science and Technology Information 10, 97–108. in Chinese with English abstract.

Yu, X.H., 1994. Cenozoic potassic alkaline ultrabasic volcanic rocks and its genesis in Lixian–Dangchang area, Gansu Province. Tethyan Geology 18, 114–129. in Chinese with English abstract.

Yu, X.H., Mo, X.X., Cao, Y.Q., Dong, G.C., 2000. Cenozoic kamafugite volcanism and its petrological characteristics west Qinling, Gansu Province. Extended Abstract for the Second World Chinese Conference A, pp. 249–254.

Yu, X.H., Mo, X.X., Liao, Z.L., Zhao, X., Su, Q., 2001. Temperature and pressure condition of garnet lherzolite and websterite from west Qinling, China. Science in China (D) S, 155–161.

Yu, X.H., Zhao, Z.D., Mo, X.X., Wang, Y.L., Xiao, Z., Zhu, D.Q., 2004. Trace element, REE and Sr, Nd, Pb isotopic geochemistry of Cenozoic kamafugites and carbonatite from west Qinling, Gansu Province: Implication of plume-lithosphere interaction. Acta Petrology Sinica 20, 483–494. in Chinese with English abstract.

Yu, X.H., Zhao, Z.D., Mo, X.X., Zhou, S., Zhu, D.Q., Wang, Y.L., 2005. $^{40}Ar/^{39}Ar$ dating for Cenozoic kamafugites from western Qinling in Gansu Province. Chinese Science Bulletin 50, 2638–2643.

Zhang, G.W., Dong, Y.P., Yao, A.P., 2002. Some thoughts on study of continental dynamics and orogenic belt. Geology in China 29, 7–13. in Chinese with English abstract.

Zhang, G.W., Zhang, B.R., Yuan, X.C., Xiao, Q., 2001a. Qinling Orogenic Belt and Continental Dynamics. Science Press. pp. 1–855. in Chinese.

Zhang, H.F., Menzies, M.A., Gurney, J., Zhou, X.H., 2001b. Cratonic peridotites and silica-rich melts: diopside-enstatite relationships in polymict xenoliths, Kaapvaal, South Africa. Geochimica et Cosmochimica Acta 65, 3365–3377.

Zhang, H.F., 2005a. Transformation of lithospheric mantle through peridotite-melt reaction: a case of Sino-Korean craton. Earth and Planetary Science Letters 237, 768–780.

Zhang, H.F., 2005b. Peridotite–melt interaction: an important mechanism for the compositional transformation of lithospheric mantle. Earth Science Frontiers 13, 65–75. in Chinese with English abstract.

Zhang, H.F., Nakamura, E., Kobayashi, K., Zhang, J., Ying, J.F., Tang, Y.J., Niu, L.F., 2007a. Transformation of subcontinental lithospheric mantle through peridotite-melt reaction: evidence from a highly fertile mantle xenolith from the North China craton. International Geology Review 49, 658–679.

Zhang, X.M., Sun, R.M., Teng, J.W., 2007b. Study on crustal, lithospheric and asthenospheric thickness beneath the Qinghai–Tibet Plateau and its adjacent areas. Chinese Science Bulletin 52, 797–804.

Zhang, H.F., Goldstein, S.L., Zhou, X.H., Sun, M., Zheng, J.P., Cai, Y., 2008. Evolution of subcontinental lithospheric mantle beneath eastern China: Re–Os isotopic evidence from mantle xenoliths in Paleozoic kimberlites and Mesozoic basalts. Contributions to Mineralogy and Petrology 155, 271–293.

Zhang, Q., Zhou, G.Q., 2001. Ophiolites of China. Science press. pp. 16–68.in Chinese.

Zheng, J.P., 1999. Mesozoic–Cenozoic mantle replacement and lithospheric thinning, East China. China University of Geosciences Press, 126. in Chinese.

Zheng, J.P., O'Reilly, S.Y., Griffin, W.L., Lu, F.X., Zhang, M., Pearson, N.J., 2001. Relics of refractory mantle beneath the eastern North China block: significance for lithosphere evolution. Lithos 57, 43–66.

Zheng, J.P., Griffin, W.L., O'Reilly, S.Y., Hu, B.Q., Zhang, M., Tang, H.Y., Su, Y.P., Zhang, Z.H., Pearson, N., Wang, F.Z., Lu, F.X., 2008. Continental collision and accretion recorded in the deep lithosphere of central China. Earth and Planetary Science Letters 269, 497–507.

Zhou, J.X., Griffin, W.L., Jaques, A.L., Ryan, C.G., Win, T.T., 1994. Geochemistry of diamond indicator minerals from China. In: Meyer, H.O.A., Leonardos, C. (Eds.), Diamonds: Characterization, Genesis and Exploration CPRM Special Publication, 1B/93, pp. 285–301.

Zhou, M.D., Lü, T.Y., Zhang, Y.S., Ruan, A.G., 2000. The geological structure background and the crustal structure in the northeastern margin of the Qinghai–Tibetan plateau. Acta Seismologica Sinica 22, 645–653. in Chinese with English abstract.